


Review

Smart Designs of Mo Based Electrocatalysts for Hydrogen Evolution Reaction

Xingyuan Gao ^{1,2} , Huilin Deng ¹, Qiuping Dai ¹, Quanlong Zeng ¹, Shuxian Qiu ^{1,*} and Xihong Lu ^{2,*}

¹ Department of Chemistry and Material Science, Engineering Technology Development Center of Advanced Materials & Energy Saving and Emission Reduction in Guangdong Colleges and Universities, Guangdong University of Education, Guangzhou 510303, China; gaoxingyuan@gdei.edu.cn (X.G.); dhuilin01@gdei.edu.cn (H.D.); daiqiuping@gdei.edu.cn (Q.D.); zengquanlong@gdei.edu.cn (Q.Z.)

² The Key Lab of Low-Carbon Chem & Energy Conservation of Guangdong Province, MOE Key Laboratory of Bioinorganic and Synthetic Chemistry, School of Chemistry, Sun Yat-Sen University, Guangzhou 510275, China

* Correspondence: qshuxian@gdei.edu.cn (S.Q.); luxh6@mail.sysu.edu.cn (X.L.)

Abstract: As a sustainable and clean energy source, hydrogen can be generated by electrolytic water splitting (i.e., a hydrogen evolution reaction, HER). Compared with conventional noble metal catalysts (e.g., Pt), Mo based materials have been deemed as a promising alternative, with a relatively low cost and comparable catalytic performances. In this review, we demonstrate a comprehensive summary of various Mo based materials, such as MoO₂, MoS₂ and Mo₂C. Moreover, state of the art designs of the catalyst structures are presented, to improve the activity and stability for hydrogen evolution, including Mo based carbon composites, heteroatom doping and heterostructure construction. The structure–performance relationships relating to the number of active sites, electron/ion conductivity, H/H₂O binding and activation energy, as well as hydrophilicity, are discussed in depth. Finally, conclusive remarks and future works are proposed.

Keywords: hydrogen evolution reaction; Mo based materials; electrocatalyst; doping; binding energy; active sites



Citation: Gao, X.; Deng, H.; Dai, Q.; Zeng, Q.; Qiu, S.; Lu, X. Smart Designs of Mo Based Electrocatalysts for Hydrogen Evolution Reaction. *Catalysts* **2022**, *12*, 2. <https://doi.org/10.3390/catal12010002>

Academic Editors:
Chelladurai Karuppiah,
Chun-Chen Yang, Shen-Ming Chen
and Prabhakarn Arunachalam

Received: 24 November 2021

Accepted: 15 December 2021

Published: 21 December 2021

Publisher's Note: MDPI stays neutral with regard to jurisdictional claims in published maps and institutional affiliations.



Copyright: © 2021 by the authors. Licensee MDPI, Basel, Switzerland. This article is an open access article distributed under the terms and conditions of the Creative Commons Attribution (CC BY) license (<https://creativecommons.org/licenses/by/4.0/>).

1. Introduction

Considering the environmental pollution and greenhouse effect caused by the excessive utilization of fossil fuels, the exploitation of renewable and clean energy sources is imminent and imperative in order to realize the sustainable development of industries and economies [1,2]. Characterized by a carbon free nature, green product (H₂O) and high energy density, hydrogen has been regarded as a promising alternative to conventional fossil fuels, prior to other renewable energies (e.g., wind and solar energy) that suffer from an intermittent nature and low energy density [3,4]. Thus far, general routes of producing hydrogen include the gasification of coal and biomass, conversion of hydrocarbons (e.g., methane and tar molecules) and electrolytic water splitting [2]. The former two methods require a high reaction temperature (i.e., intensive energy input) and exhibit a low purity of hydrogen with additional emissions of carbon dioxide [5]. In comparison, the production of hydrogen via the hydrogen evolution reaction (HER) in electrolytic water splitting enjoys zero emissions of greenhouse gases and a high hydrogen yield [6]. Particular properties of an ideal HER electrocatalyst consist of a low overpotential, low cost (scalability), high conductivity and structural stability [7]. Up to now, Pt based materials have exhibited the highest efficiency of hydrogen production; however, the limited reserves and high price essentially inhibit their utilization at an industrial level [8,9]. Recently, nonnoble transition metals have presented great potentials as an alternative to the Pt based catalysts in HER [10,11]. Among them, molybdenum (Mo) based electrocatalysts have drawn increasing interest due to their admirable activities at a wide range of pH values [12–14]. For

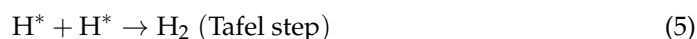
example, NiMo nanowires were constructed on Ni foam and exhibited a comparable activity to Pt/C commercial catalysts due to the metal–metal synergy and abundant active sites in the hierarchical porous structure [15]. In another case, a MoS₂ bicontinuous network was synthesized with a nanoscale size and mesoporous structure, providing more active sites for hydrogen evolution [16]. Moreover, 3 nm Mo₂C nanoparticles were highly dispersed on the carbon matrix, creating a large contact surface with the reactants and presenting considerable HER activity [17]. Other Mo based compounds (e.g., MoSe₂, MoO₂, MoN, MoP, MoB) also exhibit a good potential for producing hydrogen in high efficiencies [18–22]. Nevertheless, the sluggish reaction kinetics, because of their intrinsically low activity and poor conductivity, limit their large scale applications in HER [23]. To address the issues, various modifications have been developed to improve the catalytic performances of Mo based materials, such as combination with carbon matrix, doping with heteroatoms and construction of heterostructures [24–27]. So far, most of the reviews are focused on specific Mo based compounds; a comprehensive review based on the modification strategies of Mo based electrocatalysts rather than the materials is rarely reported in HER [1–5]. Therefore, in this review, in addition to the introduction of the reaction mechanism, all the types of Mo based materials used in HER will be summarized. Moreover, three strategies for enhanced activity and stability will be discussed in depth, including carbon/Mo based composites, heteroatom doping and the construction of heterocatalysts. The structure–performance relationships will be illustrated by referring to the physicochemical properties (e.g., active site, conductivity, hydrophilicity) and catalytic performances (e.g., overpotential and Tafel slope). Finally, conclusive remarks and possible solutions to the existing challenges will be proposed.

2. HER Mechanism

Two mechanisms are commonly recognized for HER: the Volmer–Tafel and Volmer–Heyrovsky mechanisms [1]. In acidic solutions (Equations (1)–(3) where * denotes a free site on the surface and H* denotes a hydrogen atom adsorbed on the surface), the adsorbed hydrated protons (H₃O⁺) are reduced to produce H* (intermediate) via a Volmer step; subsequently, two H* combine to form one H₂ molecule via a Tafel route or one H* reacts with the hydrated proton to form hydrogen through a Heyrovsky step.



In comparison, Equations (4)–(6) present the hydrogen evolution mechanism in neutral and alkaline electrolytes. In detail, H* is generated from the reduction of water molecules, followed by either a combination of 2 H* (a Tafel step) or the reaction between H* and H₂O (a Heyrovsky step) to produce H₂.



For both mechanisms, HER is a two step reaction, where either the Volmer step (adsorption) or the Heyrovsky/Tafel step (desorption) determines the reaction rate. Particularly, the pH of the electrolytes exerts a profound influence on the mechanism. In acidic solutions, the adsorption and electrochemical conversion of protons dominate the reaction kinetics in the Volmer step; while in neutral or alkaline conditions, the H₂O dissociation and OH[−] desorption also play a crucial role in determining the rate.

Besides, a Tafel slope is strongly related to reaction kinetics and acts as an indicator of the rate-determining step. In particular, the Volmer, Heyrovsky and Tafel steps are

reflected from the Tafel slope of 120, 40 and 30 $\text{mV}\cdot\text{dec}^{-1}$. Interestingly, under a high hydrogen coverage over 0.6, 120 $\text{mV}\cdot\text{dec}^{-1}$ a Tafel slope is also seen for the Heyrovsky step, suggesting the potential and coverage dependence of Tafel slope [28].

3. Mo Based HER Electrocatalysts

Considering the limited adsorption and desorption of hydrogen for the metallic Mo, alloying or compounding with other elements (e.g., alloys, carbides, oxides, selenides, borides, nitrides, sulfides and phosphides) effectively adjusts the electronic structure and promotes H adsorption. In addition, these Mo based materials enjoy an enhanced stability at various pH values and good electronic conductivity, benefiting the reaction kinetics and lifespan of the electrolytic HER [29,30]. In the following, different Mo based electrocatalysts will be briefly introduced by category.

The hydrogen adsorption and desorption energy of Mo metal can be adjusted by introducing other metallic elements, thus tailoring the catalytic activity for HER. Brown et al. [31] compared a series of Mo based alloys in HER and found that NiMo outperformed CoMo and FeMo. Recently, by the calcination of the NiMoO₄ precursor, the formed MoNi₄ alloy possessed a facilitated H₂O dissociation in a Volmer step in 1 M KOH electrolytes, thus presenting only a 15 mV overpotential at 10 $\text{mA}\cdot\text{cm}^{-2}$ and a 30 $\text{mV}\cdot\text{dec}^{-1}$ Tafel slope [32]. More efforts are recommended for the study of mass loading effects.

Apart from the alloys, other types of Mo based compounds have been successfully applied in HER. Owing to its good electronic conductivity, structural stability and abundant active sites (O edge and Mo edge), MoO₂ exhibits great potential as an HER catalyst. Various morphologies are synthesized to enhance the exposed active sites and inhibit agglomeration, such as nanowires, nanosheets and nanoflowers [33–37]. Another transition metal dichalcogenide—MoS₂—is widely utilized as an alternative to Pt catalysts because of earth abundance, rich active sites and chemical stability [5]. Similar with MoO₂, nearly zero differential free energy for H adsorption is achieved at the Mo and S edge [38]. A further improvement of the exposed active sites is expected for better HER activity [3]. The other dichalcogenide proven efficient in HER is MoSe₂, where the abundant exposed edge sites exhibit a higher HER activity than the inert basal plane.

In addition to combination with group VI elements (O, S, Se), a Pt like electronic structure is formed along with the d-band contraction derived from the N atom (group V element) insertion in the Mo atom interstices [39,40]. Featured with metallic behavior and thermal stability, MoN nanosheets synthesized by liquid exfoliation or the NaCl template strategy exhibited a low overpotential in both alkaline and acidic electrolytes [21]. MoP, as another representative material combining Mo and group V elements, possesses a wide range of Mo/P compositional ratios in the compounds, including Mo rich and P rich structures [41]. The electronic, structural and physicochemical properties vary with the composition. In particular, electron transfer is accelerated through the Mo–P and Mo–Mo bonds in the Mo rich MoP [42].

Mo can also form Mo_xC compounds with C (a group IV element), where the d-band of Mo is widened due to the orbital optimization of Mo and C atoms [30]. To enhance hydrophilicity and mass diffusion, a hierarchical porous structure is preferred due to the high surface area provided by micropores and fast ion transfer via the meso- and macropores [43]. In a comparison of four Mo_xC phases, the HER activity followed the order: $\beta\text{-Mo}_2\text{C} > \gamma\text{-MoC} > \eta\text{-MoC} > \alpha\text{-MoC}_{1-x}$, suggesting the different intrinsic electrochemical activities of Mo carbides [44]. Further explorations are expected to balance the adsorption and desorption of hydrogen, in order to promote the reaction kinetics in HER.

The last Mo based compounds are Mo borides (a group III element), including MoB₂, $\alpha\text{-MoB}$, $\beta\text{-MoB}$ and Mo₂B [45]. Interestingly, the Mo rich boride Mo₂B exhibited a lower HER activity than $\alpha\text{-MoB}$ and $\beta\text{-MoB}$, indicating an enhanced performance along with the increase in boron content, which was further proven by the comparable activities of Mo₂B₄ and MoB₂ [20,46]. Significantly, Mo borides with a graphene like boron layer outperformed

those with a phosphorene like boron layer, especially in acidic electrolytes. However, more investigations are suggested for catalytic behavior in alkaline solutions for Mo borides [1].

4. Smart Designs of Mo Based HER Catalysts

Despite the wide application of Mo based materials in HER, their activity and stability are still unsatisfactory due to limited active sites and sluggish electron/ion transfer. To address the issues, Mo based materials can be coupled with a conductive carbon matrix to enhance electric conductivity, the dispersion of Mo sites and specific surface area [17,47–50]. In addition, doping with heteroatoms effectively improves the intrinsic activity, lowers the kinetic energy barrier for dissociation, facilitates the charge transport and optimizes the H binding energy [26,51–54]. Moreover, the construction of heterostructures forms a synergy and benefits the HER performances [34,55]. In the following sections, the three modification strategies mentioned above for Mo based electrocatalysts will be illustrated in detail, with an in depth discussion of the structure–performance relationships in HER and a summary of the key data for representative HER catalysts in Table 1.

Table 1. Summary of the representative Mo based electrocatalysts for hydrogen evolution reaction.

Catalyst	Electrolyte	$\eta_{10}/(\text{mV at } 10 \text{ mA}\cdot\text{cm}^{-2})$	Tafel Slope/ $(\text{mV}\cdot\text{dec}^{-1})$	Ref.
NP-Mo ₂ C	0.5 M H ₂ SO ₄	210	64	[56]
Mo ₂ C/C	0.5 M H ₂ SO ₄	117	60.5	[57]
	1 M KOH	121	73.5	
Mo ₂ C/CNFs	0.5 M H ₂ SO ₄	160	66	[58]
	1 M KOH	92	63	
MoP/Mo ₂ C@C	1 M KOH	75	58	[59]
MoC-MoP/N-CNFs	0.5 M H ₂ SO ₄	158	58	[60]
	1 M KOH	137	65	
Mo ₂ C/GNR	0.5 M H ₂ SO ₄	152	65	[61]
	1 M KOH	121	54	
Mo ₂ C/N-C	0.5 M H ₂ SO ₄	155	73	[62]
	1 M KOH	78	64	
Mo ₂ C/C	1 M KOH	165	63.6	[63]
Co/Ni-MoO ₂	1 M KOH	103	80	[64]
MoO ₂ /MoS ₂ P	1 M KOH	45	64.2	[65]
	0.5 M H ₂ SO ₄	69	31	
MoO ₂ -Ni	1 M PBS	84	75.3	[66]
	1 M KOH	46	56.9	
MoP@NPSC	0.5 M H ₂ SO ₄	71	75	[67]
MoP@NCHSs	1 M KOH	92	62	[68]
CoP-MoO ₂ /MF	1 M KOH	42	127	[69]
	0.5 M H ₂ SO ₄	65	85	
MoS ₂ /MoO ₂	1 M KOH	157	119	[70]

Note: η_{10} , overpotential at 10 mA·cm⁻²; CNTs, carbon nanotubes; CNFs, carbon nanofibers; GNR, graphene nanoribbon; NCHSs, N doped carbon hollow spheres; NPSC, N, P, S codoped carbon; MF, Mo foil.

4.1. Carbon/Mo Based Composites

Coupling with a carbon matrix or additives can increase surface area, improve Mo dispersion and control particle size due to a mesoporous structure, nanoscale morphology and protective shell [56,57,71–74]. In addition, integration with conductive carbons (e.g., graphene, carbon nanotubes, and carbon black) facilitates charge transport and accelerates reaction kinetics [33,75–77]. The promotional effects of carbons on the HER performances of Mo based catalysts are elucidated in depth below.

4.1.1. Coupling with Nanoscale Carbons

Various carbon materials with nanostructures can be introduced to Mo based catalysts to achieve a high surface area and fast electron transfer, including nanotubes [76], nanosheets [78], quantum dots [79] and nanofibers [58]. For example, by carbonizing

the Mo–melamine polymer precursor on carbon nanotubes (CNTs), a high dispersion of β - Mo_2C nanoparticles and enhanced electric conductivity were both realized, delivering a much lower onset potential vs. reversible hydrogen electrode (RHE) (-195 mV for $10 \text{ mA}\cdot\text{cm}^{-2}$) than the counterpart without CNTs (-340 mV for same current density), suggesting superior electrochemical activity [74]. Moreover, a smaller Tafel slope of $75 \text{ mV}\cdot\text{dec}^{-1}$ was obtained for $\text{Mo}_2\text{C}/\text{CNT}$ than the $110 \text{ mV}\cdot\text{dec}^{-1}$ for the control sample, indicating a lower activation energy and faster reaction kinetics (Table 1). The outstanding HER performances could be attributed to the abundant active sites on the uniformly dispersed Mo_2C for H adsorption and activation, and the facilitated charge transport through the Mo_2C –CNT interfaces [59]. Owing to its merits, no decay was presented after 1000 cycles of cyclic voltammograms, demonstrating great potential as a highly durable HER catalyst in practical applications. To further immobilize the Mo_2C particles on the CNTs upon thermal treatment, oxalic acid was added to replace the ethoxy by forming oxalate groups with Mo ions (Figure 1a). Benefiting from the steric hindrance of the complex and interaction with CNTs, the Mo_2C agglomeration was considerably inhibited during the 800°C calcination, achieving a highly dispersed and small particle ($4\text{--}8$ nm) (Figure 1b) [80]. Owing to the reduced internal charge transfer resistance, the improved dispersion of active sites and large electrochemical surface area, the $\text{Mo}_2\text{C}/\text{CNTs}$ composite catalyst exhibited an overpotential of 110 mV for $10 \text{ mA}\cdot\text{cm}^{-2}$ and stable activity over 15 h and 1000 potentiodynamic sweeps (Figure 1c and Table 1). Additionally, the low Tafel slope of $51.34 \text{ mV}\cdot\text{dec}^{-1}$ suggested a Volmer–Heyrovsky mechanism, where the Heyrovsky desorption step determined the reaction kinetics [81]. Apart from the promotional effect on active site exposure by enhancing the dispersion and electric conductivity by increasing the Fermi level, the addition of CNTs exerted a profound influence on the Mo valance state. In particular, more Mo^{3+} were reduced to Mo^{2+} , so as to generate a small $\text{Mo}^{3+}/\text{Mo}^{2+}$ ratio in the presence of CNTs, which strengthened the Mo–H bond, accelerated the H_3O^+ reduction in the Volmer step and facilitated the H^* adsorption [82].

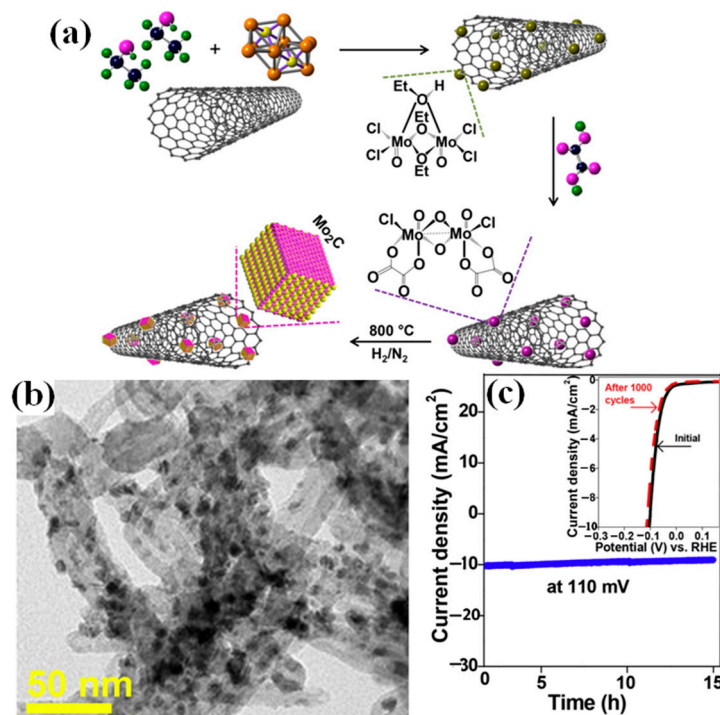


Figure 1. (a) Growth mechanism of Mo_2C on CNTs surface. (b) TEM images of oxalate derived $\text{Mo}_2\text{C}/\text{CNTs}$. (c) Time dependent profile of current density achieved under a constant 110 mV overpotential, with the inset figure of the polarization curves initially recorded and after 1000 cycles. Reproduced with permission from [81]. Copyright 2019, Elsevier.

Similar to CNTs, well defined 1D carbon nanofibers (CNFs) enjoy a moderate strength Mo–H bond, facilitated mass transport and abundant active sites [82]. Via a facile electrospinning followed by pyrolysis strategy, ultrasmall hexagonal phase Mo₂C nanocrystals (5 nm in average) were anchored in the ultralong CNFs with a diameter of 200 nm. Interestingly, a synergy was generated between the Mo₂C and CNFs. Mo₂C was well confined in the CNFs to maintain a small size during the thermal treatment and the Mo–H bonding energy was adjusted; also, the electron transfer and hydrophilicity were both promoted due to the CNF coupling [83,84]. On the other hand, the embedded Mo₂C nanoparticles enhanced the thermal stability of CNFs, which maintained their original structure after high temperature calcination, in sharp contrast to the curly morphology in the absence of an Mo source. Benefiting from synergistic effects, the Mo₂C/CNFs catalyst delivered a low overpotential at 10 mA·cm⁻² (160 and 92 mV) and a Tafel slope (66 and 63 mV·dec⁻¹) in 0.5 M H₂SO₄ and 1 M KOH, respectively (Table 1). Moreover, only a negligible overpotential shift was presented after 2000 cycles at 100 mA·cm⁻² [58]. Similarly to another work, where MoC and MoP were both embedded in the CNFs, ultrafine nanoparticles with a size of 2–7 nm were obtained after 850 °C Ar calcination, indicating a considerable confinement effect on the controlled growth of active sites [60].

In addition to 1D nanostructures, carbon quantum dots (CQDs) (less than 10 nm) act as a protective layer of MoP, to inhibit agglomeration and surface oxidation due to admirable electronic conductivity, good solubility and easy functionalization [85]. For instance, a negatively charged H₃PMo₁₂O₄₀ (HPM) precursor and positively charged ethanediamine modified CQDs (ECQDs) interacted electrostatically with each other (Figure 2a) [86]. Upon calcination, the migration, growth and oxidation of MoP were considerably alleviated by the steric hindrance of the oxo clusters and immobilization effect of ECQDs, thus achieving a small MoP size (20 nm) encircled by the CQDs (Figure 2b). Moreover, the electron transfer was promoted based on the charge polarization of Mo^{δ+} (3.1 eV peak separation in XPS Mo 3d spectra) and P^{δ-} (lower binding energy than P⁰) and low charge transport resistance (13.7 Ω), potentially benefiting the HER reaction [87]. As a result, a low overpotential of 210 mV at 20 mA·cm⁻² and small Tafel slope of 56 mV·dec⁻¹ were exhibited for MoP/CQDs (Table 1), outperforming those of pristine MoP (280 mV and 87 mV·dec⁻¹) (Figure 2c). Furthermore, negligible current degradation was presented without morphology change over 24 h and 1000 cycles [79].

A hierarchical nanostructure can form a 3D carbon network, which increases the active material loading and accelerates the charge/mass transfer through the abundant interfaces between ultrasmall Mo based particles and electrolytes [88]. For example, 3D networks consisting of carbon nanorod arrays (10 μm in length) supported on the carbon nanosheets were derived from carbonizing the biomass natural agaric, where Mo₂C nanoparticles were embedded in the carbon rod and lamellar matrices. The resulting low overpotentials of 350, 100 and 82 mV at 10 mA·cm⁻² in neutral, alkaline and acidic electrolytes, respectively, were ascribed to the enhanced diffusion of electrolytes (based on the good hydrophilicity), the abundant active sites (relating to the high surface area and Mo₂C contents in 3D complex networks), and the promoted electron/ion transfer.

4.1.2. Coupling with Graphene Based Materials

Graphene based materials, such as graphene (G), graphene oxide (GO) and reduced graphene oxide (rGO), possess a 2D nanostructure and specific properties, including a high surface–volume ratio, chemical stability and good conductivity [89–91]. Therefore, Mo/graphene based composites are introduced separately from the nanocarbon in previous sections.

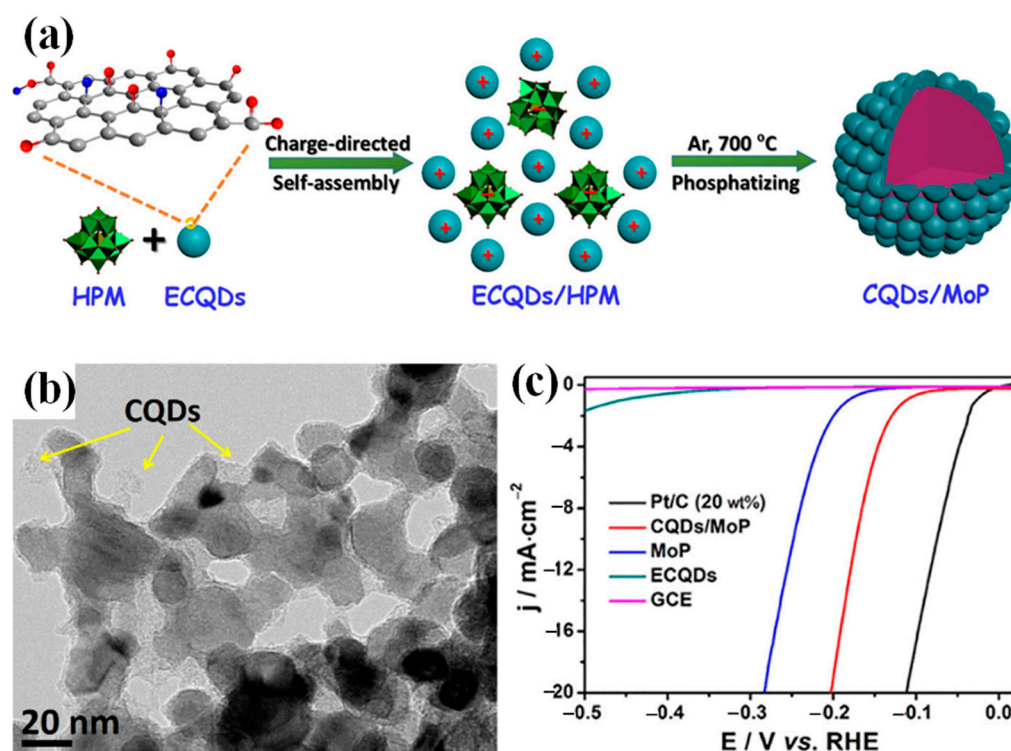


Figure 2. (a) Schematic illustration of CQDs/MoP synthesis. (b) TEM images of CQDs/MoP. (c) Polarization curves in 1 M KOH electrolyte. Reproduced with permission from [79]. Copyright 2018, American Chemical Society.

By simply mixing the GO powder and Mo precursors followed by Ar calcination, an MoO₂/Mo₂C/G composite structure was successfully prepared. The agglomeration of Mo species was effectively prevented and electron transfer was promoted with the addition of graphene, exhibiting a small Tafel slope of 59 mV·dec⁻¹. Similar promotional effects of graphene based matrices are reported for Mo₂C [92], MoS_x [75], MoO₂-Mo₂C [93], and MoP [94,95], which presented stable electrolytic HER activity in both alkaline and acidic electrolytes. To further control the size of active sites and promote exposure to reactants, a conducting MoO₂/GO membrane was derived from the carbonization of nanoballs synthesized in a template free hydrothermal method. In detail, initially, MoO₂ nanoparticles were dispersed on the GO sheets (a layer for MoO₂ nucleation and growth [90]); subsequently, the MoO₂ decorated GO sheets gradually self assembled into hollow spheres via hydrogen bonding, π - π interactions and van de Waals force [96]. The minimized MoO₂ aggregation, abundant exposed active sites, high surface area, superior structural rigidity and fast transfer of H⁺ and electrons were contributed by the formation of MoO₂/GO conducting membranes, exhibiting a much smaller Tafel slope of 52 mV·dec⁻¹ compared with the pristine MoO₂ nanoparticles (130 mV·dec⁻¹) and only a 5% current decrease after 6 h [89].

Differing from the physical mixing of the active Mo species and graphene based matrices, the in-situ formation of the composites further strengthens the interaction, and effectively anchors the active sites. In the preparation of MoO₂/rGO composites (Figure 3a), graphene as a template was first modified by poly(diallyldimethylammonium chloride) (PDDA) to be positively charged, electrostatically interacting with the negatively charged MoO₃ and facilitating the attachment of MoO₃ nanobelts on the electron rich graphene surface [97]. After annealing, MoO₃ nanobelts were in-situ reduced by H₂ and graphene, to generate a MoO₂/rGO nanocomposite. Meanwhile, rGO as an electron acceptor facilitates the charge transfer. As a consequence, a small Tafel slope of 68 mV was obtained with 70% activity retention after 1000 cycles [34]. Apart from the in-situ reduction of MoO₃ by graphene and H₂, in another case, highly dispersed Mo₂C nanoparticles were anchored in the graphene nanoribbons (GNRs) and protected by a few graphite layers via hot filament

chemical vapor deposition (HF-CVD) [61]. Particularly, H atoms derived from the H_2 and CH_4 dissociations reduced the MoO_3 directly into Mo metals without the formation of MoO_2 . Subsequently, Mo_2C nanocrystals with a size of 3–5 nm were generated by the carburization of metallic Mo. The assembled hierarchical nanostructure, where 1D Mo_2C was vertically aligned on the 2D graphene nanosheets, possessed the following merits: a small Mo_2C size, loose arrangement of active sites, high electrochemical surface area, good conductivity and moderate Mo–H binding strength. In detail, a small Mo_2C particle size exposed a high active surface to the reactants, increasing the electrocatalytic activities in HER [98]. Additionally, Mo_2C nanocrystals were loosely distributed and covered in the graphene nanosheets, enabling H_2 release from the catalyst without harm. Moreover, the enhanced active surface area could be measured based on the capacitance (Figure 3b) that the Mo_2C /GNRs exhibited a much higher capacitance of $23.34 \text{ mF}\cdot\text{cm}^{-2}$ than that of the pristine Mo_2C ($0.42 \text{ mF}\cdot\text{cm}^{-2}$). Correspondingly, Mo_2C /GNRs possessed a significantly rougher surface, with a factor of 1060, than the naked Mo_2C (19). Furthermore, d-band centers shift downwards along with the charge transfer from Mo_2C to graphene, which reduced the Mo–H bonding energy and promoted the desorption of H^* , thus improving the reaction kinetics of HER [99]. Notably, the relative inert graphene could be activated by Mo_2C that the H adsorption free energy reduced from 1 to 0.3 eV (Figure 3c). Owing to the above merits, Mo_2C /GNRs delivered a lower overpotential in alkaline (121 mV) and acidic (152 mV) electrolytes at $10 \text{ mA}\cdot\text{cm}^{-2}$ than those of the counterpart (266 and 275 mV, respectively) (Table 1). On the other hand, a smaller Tafel slope was also presented in both solutions for Mo_2C /GNRs, with a negligible current density drop shown after 30,000 s in both electrolytes, demonstrating a superior electrocatalytic activity and stability over a long term operation [61].

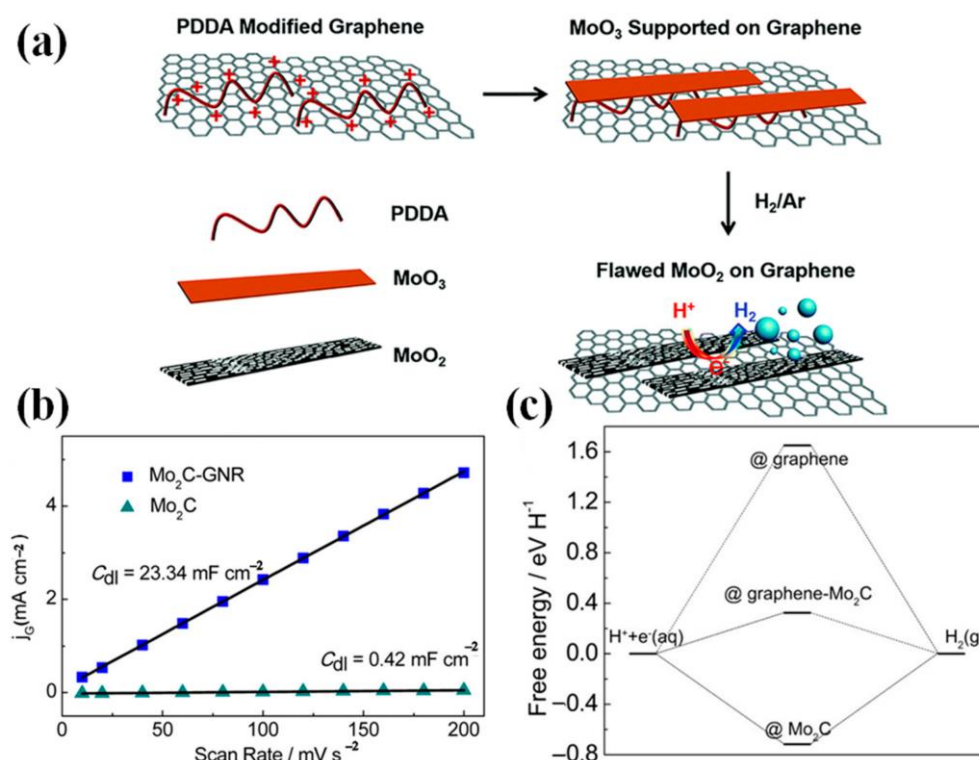


Figure 3. (a) Preparation scheme of the MoO_2 on graphene. Reproduced with permission from [34]. Copyright 2015, The Royal Society of Chemistry. (b) Current density plotted against scan rate. (c) Free energy evolution of H, against standard hydrogen electrode (SHE). Reproduced with permission from [61]. Copyright 2017, American Chemical Society.

4.1.3. Coupling with Mesoporous Carbons

By combination with mesoporous carbon matrices, the contact surface between the Mo based electrode and electrolyte was enlarged, improving the transfer of charge and mass [50]. Generally, a mesoporous structure presents a type IV isotherm of N₂ adsorption/desorption, with a large slope at high pressure regions [100]. In addition, the average pore size ranges from 2–50 nm. With such a specific structure, the electrocatalyst possesses a fast diffusion of electrolytes and high active surface for the adsorption and activation in HER [101]. For example, via the thermal carbonization of sunflower seed shells, a mesoporous carbon matrix with a high specific surface area (401.5 m²·g⁻¹) and average pore size (3.9 nm) was produced for the homogeneous distribution of Mo₂C nanoparticles (5–8 nm) [102]. The higher HER performances were attributed to the boosted electron transfer rate and interfacial reaction kinetics, which resulted from the large surface area and abundant mesopores [103]. To further enhance the reaction kinetics, a mesoporous carbon matrix with a 3D architecture was prepared by the calcination of ammonium heptamolybdate and rice paper. Owing to the fast diffusion of charge/mass through the channel rich interfaces, large exposed surface area and abundant active sites for adsorption and reaction, the Mo₂C embedded in 3D mesoporous carbons exhibited a low overpotential of 155 and 78 mV at 10 mA·cm⁻² and a small Tafel slope of 73 and 64 mV·dec⁻¹ in 0.5 M H₂SO₄ and 1 M KOH, respectively, with a stable catalytic activity over 10 h and 2000 runs (Table 1) [62].

In addition to the preparation of mesoporous carbons from natural products and textiles, metal–organic frameworks (MOFs), as a precursor, can offer a confined environment with abundant pores generated by organic ligands. In particular, an Al-MOF (MIL53) was hydrothermally synthesized and possessed a microporous structure based on the type I curves of adsorption/desorption [104]. Benefiting from the large surface area (1165 m²·g⁻¹), MoCl₅ was homogeneously impregnated in the MOF frameworks. During the carbonization, Mo₂C was in-situ formed from the reduction of Mo species under CH₄ decomposition (Figure 4a). Meanwhile, the microporous MOFs collapsed into a rigid and mesoporous structure (type IV behavior in BET and pore size of 3.6 nm). As a result, the nucleation and growth of β-Mo₂C nanocrystals were considerably inhibited by the mesoporous texture and confined space of the MOF derived carbon matrix, producing a small and highly dispersed Mo₂C with the size of 5–10 nm, while those prepared with commercial carbon support possessed a much larger size of 20–40 nm. The carbon layers not only protected the Mo₂C from agglomeration during high temperature calcination, but also facilitated electron transfer and H₂ gas release from the system (Figure 4b). Following the Volmer–Heyrovsky mechanism, the β-Mo₂C/C composite electrocatalyst presented a 165 mV overpotential at 10 mA·cm⁻² and a Tafel slope of 63.6 mV·dec⁻¹, outperforming the Mo₂C/commercial carbon (229 mV and 74.5 mV·dec⁻¹) (Figure 4c) [63].

Compared with mesopore alone, a hierarchical porous structure generates a synergy of macropore and mesopores. Particularly, mass diffusion is facilitated through the macropores and abundant active sites are exposed in the mesopores [105]. By the facile impregnation carbonization of the ammonium heptamolybdate (Mo precursor), F127 (surfactant), resorcinol and formaldehyde, Mo₂C was formed in-situ since the carbon source was partially consumed, which was reflected by the increase in mesopore size from 4.8 to 5.6 nm. Moreover, homogeneous macropores (9 μm) and ordered mesopores (5.6 nm) coexisted after the thermal treatment, proven by an Hg intrusion test [106]. Anchored in the wall of mesopores, the migration and growth of Mo₂C nanocrystals were limited, producing an ultrasmall particle size of 5 nm. In turn, the embedded Mo₂C nanoparticles improved the hydrophilicity based on the reduced water contact angle (80.4° vs 119.8°). The combination of macropores and good wettability enabled a fast and efficient electrolyte diffusion and the escape of gas products. As a consequence, a low overpotential of 230 mV was delivered to generate a high current density of 500 mA·cm⁻². The small Tafel slope of 63 mV·dec⁻¹ indicated an outstanding HER activity and Volmer–Heyrovsky mechanism [107].

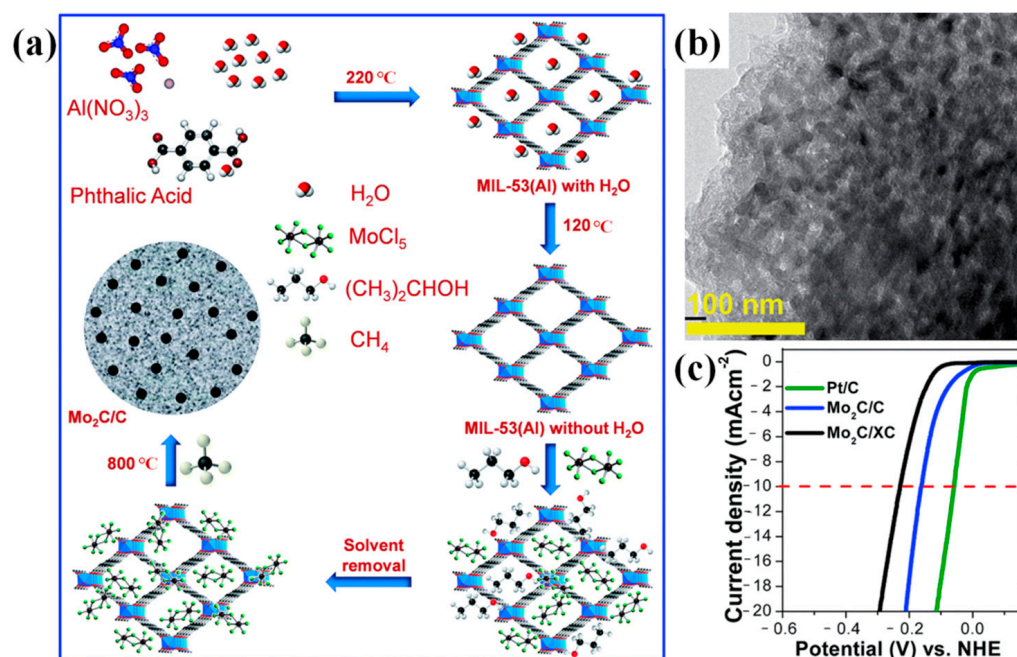


Figure 4. (a) Formation scheme of Mo₂C/C electrocatalyst. (b) TEM of Mo₂C/C. (c) Current–potential profiles of Pt/C, Mo₂C/C and Mo₂C/XC72. Reproduced with permission from [63]. Copyright 2016, The Royal Society of Chemistry.

4.1.4. Core Shell Structure

To protect Mo species from agglomeration, oxidation and corrosion (etching), a core shell structure is developed with carbon layers as the shell covering the Mo based compounds [57,83,108]. Meanwhile, the presence of the carbon shell promotes the charge transfer through the electrode–electrolyte interfaces [109]. For example, when Mo₂C particles were embedded in the 3D carbon network and encapsulated by the carbon shell, they interacted intimately with the carbon matrix and were separated from direct contact with the electrolytes, thus facilitating electron transfer and inhibiting corrosion [57]. Moreover, the size of the Mo₂C was only 2–2.5 nm due to the confinement effect of the carbon shell, possessing a large amount of active sites exposed to the reactant. Thus, in acidic and alkaline electrolytes, a low overpotential of 117 and 121 mV were needed to obtain 10 mA·cm⁻² current density (Table 1). In addition, the small Tafel slope of 73.5 mV·dec⁻¹ indicated a fast kinetics in HER, benefiting from the high electrochemical active area based on capacitance [110] and low internal charge transfer resistance [57].

In the above work, the application of Polyoxometalates (POMs) has been proven a good precursor to generate highly distributed Mo based particles due to their diverse structures and unique composition [108]. To realize a better dispersion of the POMs, dicyandiamide (DCA) was mixed with the precursor; after calcination, graphitic carbon layers were formed, covering MoP/Mo₂C nanoparticles to protect them from aggregation (Figure 5a) [108]. Moreover, the carbon shells reduced the charge transfer resistance at the interface between the electrocatalyst and electrolyte, reflected from the small R_{ct} (7.08 Ω) based on the EIS test (Figure 5b). Owing to the above merits, an MoP/Mo₂C@C core shell catalyst exhibited a low overpotential of 75 mV to achieve 10 mA·cm⁻² current density at 1 M KOH (Table 1). In addition, the admirable stability over 1000 cycles and 14 h operation was attributed to the strong resistance to agglomeration and etching with the protective carbon layers (Figure 5c) [59]. Similar findings were also reported in Mo₂C@C, which possessed a superior performance in HER [111].

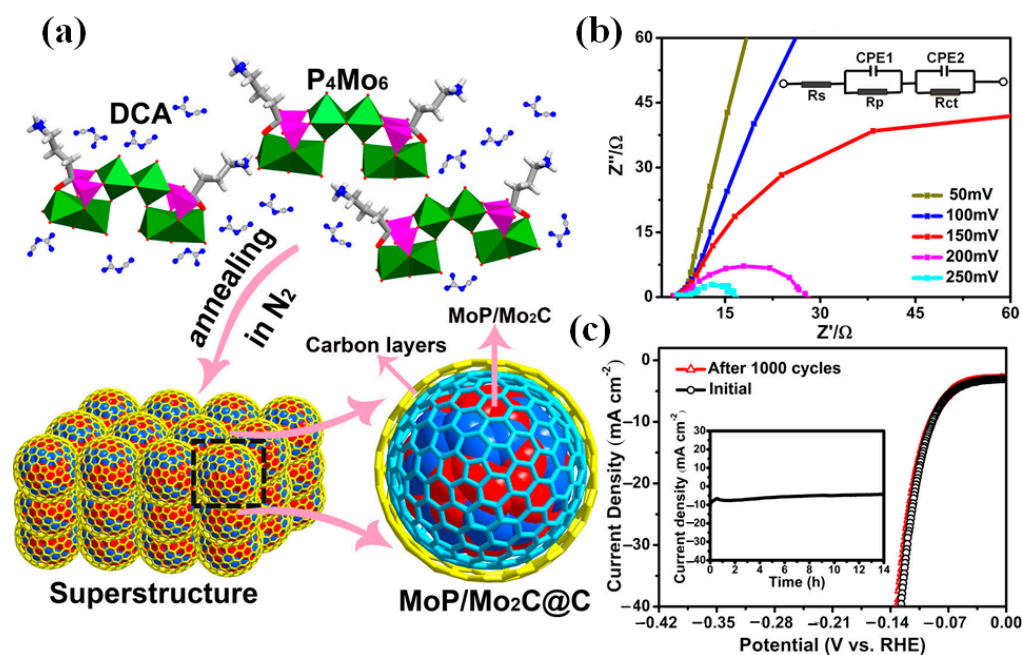


Figure 5. (a) Preparation scheme of MoP/Mo₂C@C. (b) Nyquist plots of electrochemical impedance spectra (EIS). (c) Polarization curves of MoP/Mo₂C@C. Inset: Time dependent current density curve under a constant overpotential of 60 mV. Reproduced with permission from [59]. Copyright 2017, American Chemical Society.

4.2. Heteroatom Doping

Nonmetallic (e.g., N, P, S, C) and metallic (e.g., Ni, Co) elements can be doped in the Mo compounds and carbon matrices to enhance the electrocatalytic properties in HER by increasing the number of active sites, tuning electron structure, facilitating electron transfer, improving hydrophilicity, promoting H^{*} adsorption/desorption and stabilizing the Mo sites [56,64,65,75,112–114]. In the following sections, the doping effects of heteroatoms will be introduced by category, including nonmetallic atom doping (single element [74,115–119], dual elements [103,117,120,121] and triple elements [122]) and metallic atom doping [64,66,72].

4.2.1. Nonmetallic Atom Doping

Single Atom Doping

Owing to the strong electronegativity and lone pairs, nonmetallic atoms (e.g., N, S, P, C) can activate the carbon matrix, introduce structural defects and weaken Mo–H bonds, thus stabilizing the Mo species, increasing the active center amount, enhancing electronic conductivity and facilitating H₂ release [56,57,67,112,113,119,123,124]. As for the N doping, abundant Mo²⁺ sites are produced and Mo–H binding is moderated by Mo–N interactions [60]. Electrons are withdrawn by N atoms and H₂ is easily activated [125]. In addition, the surface electronic structure is reconstructed to form an activated carbon matrix [126]. Specifically, the carbon nanolayers coupled with N atoms become wrinkled and rough, and sp² hybrid orbitals are changed, which generates a nearly zero Gibbs free energy, thus promoting H adsorption [88]. Moreover, the carbon substrate doped with N possesses n-type and metallic character, benefiting electron transfer [127]. For example, Mo₂C nanosheets doped with N were synthesized via chemical vapor reduction with dicyandiamide as the N source [123]. Based on the characteristic peaks of Mo²⁺ at 231.6 and 228.6 eV (Mo 3d spectra) and pyridinic N at 398.5 eV (N 1s spectra), the successful introduction of N and the electron rich environment surrounding Mo were proven [4]. Benefiting from the lone pairs of N atoms, the adsorption of active H was promoted and electronic conductivity was enhanced with an increased spin density and electron density [125]. In addition, more active sites were exposed with the manipulation of electron

density states by N atoms. Thus, a low overpotential of 99 mV at $10 \text{ mA}\cdot\text{cm}^{-2}$ and a small Tafel slope of $44.5 \text{ mV}\cdot\text{dec}^{-1}$ were realized for N doped Mo_2C nanosheets [123]. The detailed mechanism was elucidated based on a DFT calculation [112]. The lone pair electrons of the N atom modulated the electronic structure of the neighboring Mo and C atoms and enabled an intimate interaction with protons and water [128]. Compared with the -1.57 eV Gibbs free energy of H atom adsorption for undoped MoC, the ΔG_{H^*} of N doped MoC was only -0.32 eV , much closer to zero, which suggested a facilitated electron/proton transfer and hydrogen release [112]. However, excessive N doping possibly inhibited electron transport from MoC to the underlying materials during H_2O activation, and subsequent OH^- adsorption [129].

Different N configurations were compared regarding their contributions to the HER activity of N doped MoP@carbon, including pyrrolic N, pyridinic N and graphitic N [68]. In the preparation, N atoms were introduced by the oxidative polymerization of pyrrole initiated by $\text{H}_3\text{PMo}_{12}\text{O}_{40}\cdot n\text{H}_2\text{O}$ (an Mo precursor). After calcination and phosphidation with the help of polystyrene spheres as the sacrificial template, MoP nanoparticles were encapsulated within the hollow N doped carbon spheres (Figure 6a). After peak fitting, the N 1s spectra were deconvoluted into four configurations (pyridinic N at 397.8 eV, pyrrolic N at 400.5 eV, graphitic N at 401.4 eV and pyridinic N–O at 402.5 eV) (Figure 6b) [130]. Compared with graphitic carbon, H_2O adsorption was facilitated in pyridinic and pyrrolic N atoms due to their stronger electron-withdrawing property (Figure 6c). Moreover, MoP coupled with pyridinic N possessed a lower dissociation energy barrier for H_2O than the pyrrolic N, promoting the proton generation in Volmer step (Figure 6d). Notably, a combined doping with pyridinic and pyrrolic N exhibited the smallest ΔG_{H^*} , enhancing the evolution of H_2 in the subsequent Heyrovsky step. To further elucidate the dominated contribution of pyridinic N [131], the adsorption energy of OH^* was compared. It turned out that the ΔE_{OH^*} of the pyridinic N was 2.84 eV, much higher than that of graphitic N (-0.41 eV) and pyrrolic N (1.84 eV), significantly facilitating the $-\text{OH}$ desorption and preventing the active sites from being covered by the re-adsorbed water molecules (Figure 6e) [132]. Owing to the electron rich N atoms, lower d-band center, weakened Mo–H bond, more structural defects at grain boundaries, abundant Mo–N bonds on the surface and proper balance between OH^* adsorption/desorption, the highly active pyridinic-N-MoP sites resulted in a low overpotential of 92 mV at $10 \text{ mA}\cdot\text{cm}^{-2}$ [68,133].

Similar to N doping, the introduction of P atoms can modulate the electronic structure and surface electron state of a carbon matrix and Mo compounds, which improves conductivity and optimizes H adsorption, thus enhancing reaction kinetics [65,134]. When P was doped into MoS_2 , defects were generated in the disordered hexagonal structure of the MoS_2 basal plane, acting as the active sites for HER. Meanwhile, Mo bridges (e.g., O–Mo–P and O–Mo–S) with a shorter bond length benefited the electron transfer at the interface [65]. The doping concentration of P greatly influenced the intrinsic activity and HER kinetics. At a P/S ratio of 0.14, the Gibbs free energy of H adsorption was only 0.24 eV, consistent with the better HER performances. Specifically, the electron density of S was reduced because of the electron transfer from Mo to P, so as to regulate the adsorption and desorption of H^* [135]. In comparison, excessive P doping lowered the intrinsic activity of MoS_2 by breaking the structure. Thus, the appropriate amount of P atoms enabled a balance between the H_2O dissociation and H desorption. On the other hand, a narrower bandgap of 1.58 eV was obtained by P doping, compared with the pristine MoS_2 (1.84 eV). Meanwhile, more charge carriers were generated based on more electron states near the Fermi level and the appearance of new bands. Owing to the merits above, a small overpotential of 45 mV was delivered, to achieve $10 \text{ mA}\cdot\text{cm}^{-2}$ in alkaline electrolytes (Table 1) [65].

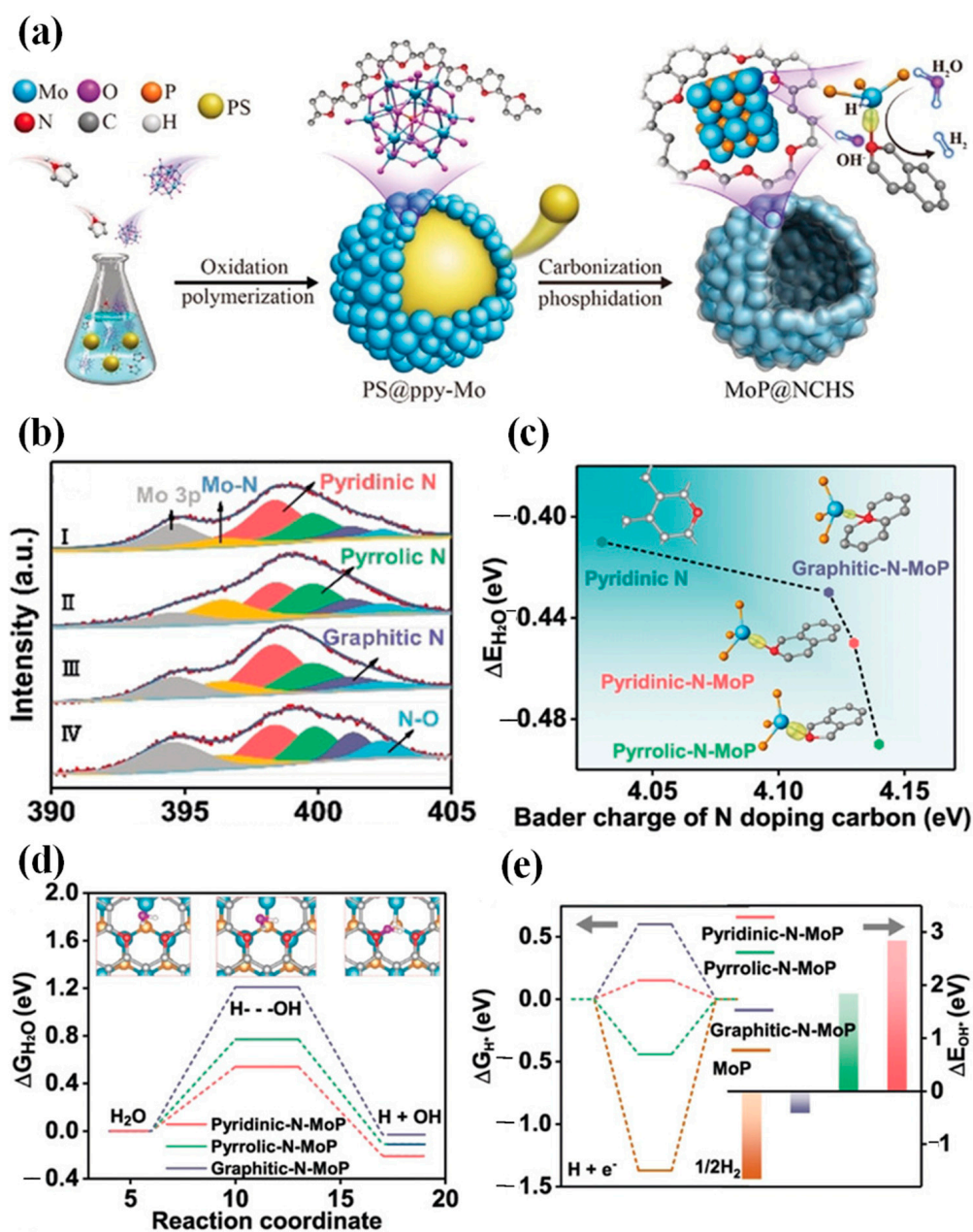


Figure 6. (a) Fabrication schematic of MoP@NCHS. (b) XPS spectra of N 1s. (c) Average Bader charge of N doped carbon. (d) Free energy diagram of the water dissociation at pyridinic-N-MoP. (e) Chemisorption energies of OH* (right). Reproduced with permission from [68]. Copyright 2020, Wiley.

Dual Atoms Doping

Compared with single nonmetallic atom doping, dual atoms doping enjoys the synergy between the two dopants in HER. When N, P or N, S were codoped into Mo₂C/C by precipitation, carbonization and hydrothermal treatment with phosphomolybdic acid (P source), dicyandiamide (DCA, N source) and thioacetamide (TAA, S source) (Figure 7a), the newly formed hybrids possessed a larger active area for reaction, higher intrinsic activities, lower internal electronic resistance and enhanced wettability by increasing the polarity and modulating the Mo₂C d-orbitals [56,136]. Benefiting from the modulated electronic structures and improved HER kinetics, the dually doped sample (NP- and NS-doped) exhibited a lower overpotential than a single N doped counterpart (210 and 213 vs. 265 mV at 10 mA·cm⁻²) (Figure 7b) [56]. In addition, based on the Tafel slope (64 and 44 vs.

$78 \text{ mV}\cdot\text{dec}^{-1}$) (Figure 7c and Table 1), the reactions all followed the Volmer–Heyrovsky mechanism and the Volmer step determined the overall rate. More importantly, the smaller slopes for the dual atoms doping suggested a faster HER kinetics resulting from moderate Mo–H bonding and abundant active centers for diffusion, adsorption and reaction [137].

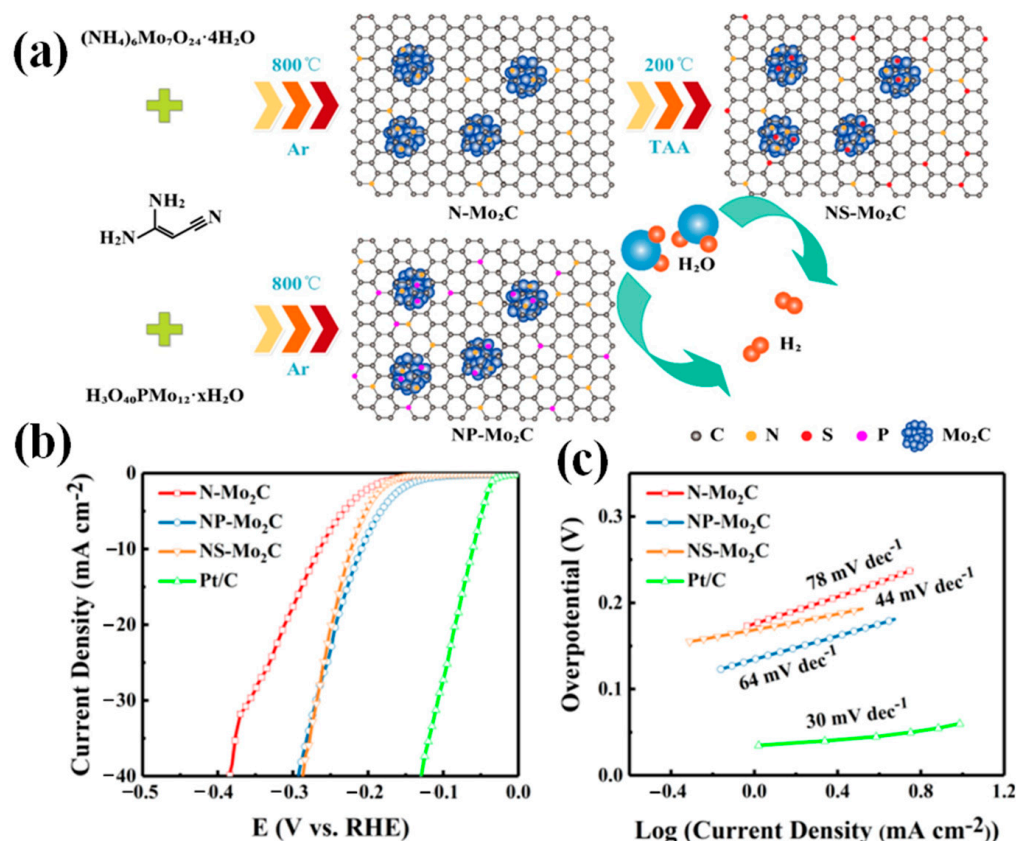


Figure 7. (a) Synthesis scheme of NP-Mo₂C and NS-Mo₂C. (b) Polarization curves. (c) Tafel plots. Reproduced with permission from [56]. Copyright 2018, Elsevier.

The synergistic effects of dual doping are also reported in other works. In a series of couples (P–S, P–N, P–C), the electron transfer from P to the Mo sites via the other dopant was greatly promoted, stabilizing the MoP, offering more adsorption sites of H⁺ and presenting better electronic conductivity [75,92,138]. In another case, MoC possessed a higher Fermi level with the codoping of N and P, facilitating the reduction in hydrated protons at the beginning step of HER [139]. In comparison to the single N doped MoC, N, P- or N, S codoped MoC exhibited a lower ΔG_{H^+} [140]. Lan et al. [57] also doped N and P into Mo₂C nanoparticles embedded in a carbon matrix, and found that the doping enhanced the reaction kinetics and provided more adsorption sites for reactants. Based on the C_{dl} values, dually doped Mo₂C/C possessed a much higher electrochemical active surface area ($20.1 \text{ mF}\cdot\text{dec}^{-1}$) than the single doped and undoped samples (15.3 , 10.5 and $7.3 \text{ mF}\cdot\text{dec}^{-1}$).

Triple Atoms Doping

It is well known that doping with nonmetallic heteroatoms (e.g., N, P, S) onto carbon matrices enables a fast electron and ion transport, modulates electron density and adjusts hydrogen binding energy [141–143]. Simultaneous doping of the above elements could further modify the electronic structure and enhance the reaction kinetics in HER [142]. By codoping N, P and S into the porous carbon matrix for MoP, abundant active sites were also generated for adsorption, thus leading to a low overpotential of 70 mV at $10 \text{ mA}\cdot\text{cm}^{-2}$, with a Tafel slope of $87.2 \text{ mV}\cdot\text{dec}^{-1}$ and no obvious shift of current density over 12 h [122].

To further improve the morphology of Mo species and interaction with the carbon matrix, N, P and S heteroatoms were doped with egg white (S and N source), phosphomolybdic acid (Mo and P source) and NaH_2PO_2 (P source) via hydrothermal, followed by thermal calcination [67]. In the preparation process, proteins in the egg white promoted the assembly with $\{\text{PMo}_{12}\}$ clusters through hydrogen bonds, forming an inorganic–organic hybrid precursor; after being treated with NaH_2PO_2 , small MoP flakes were coated by a thin layer of N, P, S doped carbon, proven by the XPS spectra of C–N, C–S and C–P bonds [144]. With this multiple doping, the spin density was adjusted and the adsorption energies of H and –OH were tailored [145]. Meanwhile, the intimate contact between the MoP flakes and multiatom doped carbon enhanced the electron transfer [146]. Owing to the good electronic conductivity, abundant active centers and efficient ion transfer, low overpotentials were delivered in acid (71 mV), neutral (76 mV) and alkaline (50 mV) electrolytes at $10 \text{ mA}\cdot\text{cm}^{-2}$ with a nearly constant operation over 40 h [67].

4.2.2. Metallic Atom Doping

Similar to nonmetallic atom doping, various metal elements (e.g., Ni, Co) can be doped in Mo based catalysts to improve HER activity and stability by modulating the electronic structure, enhancing conductivity, tuning the binding energy of H and producing more active sites [147–149]. For example, Hu et al. [72] doped Ni into an Mo_2C /carbon fiber paper hybrid and found that the resistance to charge transfer decreased from 12.7 to 9Ω compared with an undoped counterpart. More importantly, a good balance was struck between the adsorption and desorption of H on/from the Mo_2C by changing the valence state of Mo [137]. Thus, a low overpotential of 121.4 mV at $10 \text{ mA}\cdot\text{cm}^{-2}$ was exhibited with a 10-h stable operation [72]. To promote the electronic interaction between Ni and Mo, Ni was first electrodeposited on carbon cloth (CC) followed by preparing the Ni–Mo precursor by the hydrothermal treatment of molybdate; after calcination, an Ni– MoO_2 /CC hybrid catalyst was formed [66]. Based on the positive shift to 855.8 eV (Ni– MoO_2) from 854.7 eV (Ni) in a Ni 2p XPS spectra, a strengthened interaction was suggested by the electron transfer from Ni to Mo [148]. Due to the strong Ni–Mo interaction, the O 2p orbitals in MoO_2 were upraised, thus facilitating the hydrogen adsorption [150]. In the meantime, water adsorption and dissociation were improved on the positive charged Ni species, further enhancing the H adsorption on MoO_2 . The modified metal–H bonds could interact with H_2O molecules and electrons to release H_2 via the Heyrovsky step (neutral and alkaline electrolytes) and Tafel recombination step (acidic electrolyte) [151]. As a result, this robust HER catalyst presented a low overpotential of 84, 69 and 46 mV at $10 \text{ mA}\cdot\text{cm}^{-2}$ in neutral, acidic and alkaline electrolytes with a superior stability over 36 h in all pH ranges [66].

Apart from Ni doping, the dual atoms doping of Ni and Co synergistically optimizes the metal–H binding energy and facilitates electron transport. Via a facile physical mixing and calcination, Co, Ni codoped MoO_2 possessed a homogeneous dispersion of Co, Ni, Mo and O elements. The weak Co–H and Ni–H bonds modulated the hydrogen adsorption and desorption behaviors. In addition, a larger electrochemical active area was enabled for codoped MoO_2 , based on the higher C_{dl} value of $7.7 \text{ mF}\cdot\text{cm}^{-2}$, than the single doping (5.5 and $5.6 \text{ mF}\cdot\text{cm}^{-2}$ for Co- and Ni- MoO_2 , respectively). Moreover, benefiting from the optimized electronic structure, charge transfer resistance was reduced with the dual doping, favoring a fast HER kinetics [152,153]. As a consequence, the overpotential to achieve $10 \text{ mA}\cdot\text{cm}^{-2}$ was smaller for Co, Ni codoped MoO_2 (103 mV) in comparison to Co- MoO_2 and Ni- MoO_2 (Table 1) [64].

4.3. Heterostructure Construction

Compared with the single Mo based materials applied in HER (e.g., MoP, MoS_2 , Mo_2N , Mo_2C and MoO_x), heterostructures constructed by different Mo species possess a synergy, such as balanced H adsorption and desorption, promoted H_2O adsorption and dissociation, mass/electron transfer ability, abundant active sites, high electrochemical surface area and

enhanced intrinsic activities [59,65,93,154–156]. For example, MoO₂ is featured with good electronic conductivity, high chemical stability and abundant active sites (Mo and O edges), thus being widely studied as a HER catalyst [93,157,158]. By forming a heterostructure with CoMo, the positive ΔG_{H^*} (0.15 eV) of MoO₂ was complemented by the negative values of Co (−0.27 eV) and Mo (−0.37 eV) [159], improving the intrinsic HER activity at the metal/metal oxide interface [160]. Benefiting from the stabilized Mo⁴⁺ by the insoluble Mo species and the abundant active sites, a low overpotential of 76 mV at 50 mA·cm^{−2} was delivered [161]. Apart from CoMo, coupling with CoP and Mo foil enabled an optimized hydrogen adsorption capability in the presence of P sites and charge redistribution at the interface of heterostructures. Owing to the ultralow ΔG_{H^*} (0.02 eV) and promoted H₂O adsorption, the overpotential to drive 10 mA·cm^{−2} was only 42 mV (Table 1) [69]. Based on a DFT analysis, the possible mechanism was proposed that H₂O dissociated from the hydrophilic MoO₂ surface; subsequently, the produced H adsorbed onto the nearby P sites to combine with H₂O to release H₂ from CoP surface. Both the Volmer and Heyrovsky steps were accelerated at the heterointerfaces [162,163].

Besides integration with Mo metals and CoP, since MoS₂ enjoys a low cost and special structure, with S edges as the active centers [164], MoO₂–MoS₂ heterojunction may generate a synergy in the HER process. By vertically growing MoS₂ nanosheets onto MoO₂ nanobelts, the stacking of S–Mo–S interlayers was alleviated, exposing more active sites and facilitating electron transport [165]. Compared with MoS₂ (230 mV) and MoO₂ (280 mV), a much lower onset potential of 120 mV (vs. RHE) was delivered for MoS₂/MoO₂ heterocatalyst [119]. Notably, the ratio of MoO₂ and MoS₂ determined the HER activity. In particular, with the optimal ratio of 10:1, the smallest Tafel slope of 46 mV·dec^{−1} and a negligible activity drop over 5000 cycles were achieved owing to the lowest internal electron transfer resistance (121 Ω) and largest electrochemical surface area/amount of active sites ($C_{dl} = 7.22 \text{ mF}\cdot\text{cm}^{-2}$) [155,166]. In comparison, a higher ratio (excessive MoO₂) inhibited the adsorption/desorption of molecules and ions and a lower ratio (excessive MoS₂) deteriorated the HER activity due to hindered electron transfer, thus slowing down H₂ production via proton recombination [155].

Differing from the sulfidation of Mo oxides, Huang et al. [70] partially oxidized MoS₂ to form a MoS₂/MoO₂ hybrid HER electrocatalyst with Fe₂O₃ as the redox agent and hard template in the solid phase reaction route. In particular (Figure 8a), tiny Fe₂O₃ nanoparticles were initially anchored on the MoS₂ basal plane; under thermal treatment in N₂, oxygen atoms were released from Fe₂O₃ to convert the MoS₂ into MoO₂ and SO₂ with the simultaneous formation of Fe₃O₄; after acid etching, porous MoS₂/MoO₂ heterostructure was generated with abundant active centers (e.g., Mo, O, S), exhibiting a synergy for reactant adsorption, dissociation, activation and desorption in a fast kinetics [36,167]. Interestingly, both the calcination temperature and Mo/Fe ratio significantly affected the catalytic performances. As shown in Figure 8b, the lowest overpotential was delivered at an annealing temperature of 550 °C; at a higher temperature (e.g., 600 °C), the drop in catalytic property might result from the exceedingly high crystallinity (Table 1). On the other hand, an appropriate oxygen concentration was obtained with a Mo/Fe ratio of 7:3, which presented the highest current density and largest electrochemical surface area (ECSA) of 196 cm^{−2} (Figure 8c) [70].

To facilitate electron transport and increase the ECSA of MoS₂, coupling with MoN was proven effective in creating more active sites and modulating the hydrogen binding energy [168]. With the help of C₃N₄, a MoS₂/MoN heterostructure was constructed via hydrothermal and thermal annealing [154]. The strengthened interface interaction was confirmed by XPS spectra where more apical and bridging S ligands were generated than the edge/terminal ones [169]. Following the Volmer–Heyrovsky mechanism based on the Tafel slope (59 mV·dec^{−1}), the heterocatalyst exhibited a low overpotential of 57 mV at 10 mA·cm^{−2} [154]. Similarly, integrating MoS₂ with Mo₂C and Co₉S₈ generated tremendous amounts of interfaces with abundant active sites and higher inherent conductivity for electron transfer. Based on the DFT calculation, ΔG_{H^*} was greatly reduced, from

5.31 eV (MoS_2) to 1.99 eV (heterostructure), promoting hydrogen evolution with a 174.2 mV overpotential at $10 \text{ mA}\cdot\text{cm}^{-2}$ [76].

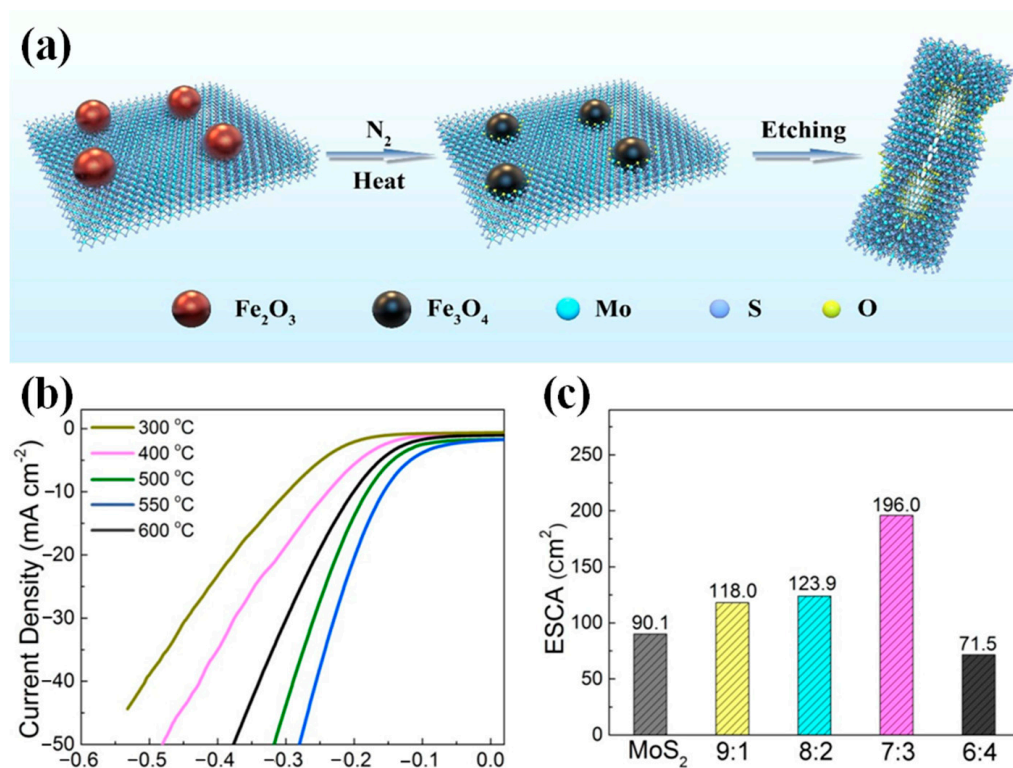


Figure 8. (a) Preparation scheme of porous $\text{MoS}_2/\text{MoO}_2$ hybrid. (b) HER polarization curves of the $\text{MoS}_2/\text{MoO}_2$ samples annealed at different temperatures. (c) Electrochemical surface areas (ECA) of $\text{MoS}_2/\text{MoO}_2$ with different Mo/Fe molar ratios (9:1, 8:2, 7:3, and 6:4). Reproduced with permission from [70]. Copyright 2020, Elsevier.

In addition to the $\text{MoS}_2\text{-Mo}_2\text{C}$ couple, MoO_2 and Mo_2C can also be integrated to form a heterostructure, combining the unique properties of Mo_2C at all pH ranges and good conductivity of MoO_2 [170]. Abundant active sites and electron transport paths were generated from the $\text{MoO}_2/\text{Mo}_2\text{C}$ heterojunction, benefiting hydrogen adsorption and desorption behaviors [171]. The resulting enhanced intrinsic activity was reflected from the large exchange current density ($6.8 \times 10^{-2} \text{ mA}\cdot\text{cm}^{-2}$) [73]. MoC was also coupled with MoP to generate a strong interfacial interaction, which promoted the formation of ultrafine heterostructure MoC/MoP nanoparticles with a good antioxidation property. Due to the modulated Mo^{2+} electron density and H binding energy, the inherent activity was considerably enhanced, thus delivering a high exchange current density of $8.5 \times 10^{-3} \text{ mA}\cdot\text{cm}^{-2}$. With the optimal ratio of MoC and MoP , the desorption of H and reduction of proton were well balanced [82], obtaining a low overpotential of 158 and 137 mV to drive $10 \text{ mA}\cdot\text{cm}^{-2}$ in acidic and alkaline electrolytes, respectively [60].

5. Conclusions and Prospects

In this review, a comprehensive summary of the recent development of Mo based electrocatalysts for the hydrogen evolution reaction (HER) is demonstrated. The fundamentals of HER and representative Mo compounds catalysts are introduced at first, and main contents are state of the art modifications of the Mo based structures. Particularly, by coupling with carbon nanostructures, doping with heteroatoms (nonmetallic and metallic elements), and constructing heterostructures, HER activity and stability are both enhanced. The improved performances can be attributed to the modulated adsorption, conversion and desorption of reactants and intermediates, the faster transport of electrons and ions,

improved wettability and increased number of active sites. Despite existing progress, several issues are still waiting for a possible solution.

First, more efforts are expected to further enhance the HER performances of Mo based catalysts to satisfy large scale applications in industry. Recent advanced preparation strategies, such as MOF assisted synthesis and single atom structures, might be a promising option. Meanwhile, to realize the industrialized production of hydrogen, the cost of raw materials and simplicity of the synthesis procedures need special consideration.

Second, the detailed catalytic mechanisms that have been proposed for Mo based heterostructures with/without doping are not clear enough. More efforts are recommended to elucidate the structure–performance relationships and the origin of active sites, relying on theoretical studies and advanced characterization techniques.

Third, to achieve a balanced and optimal water splitting performance, the electrocatalyst design should enable a robust activity in all pH ranges, especially for HER in alkaline solutions and OER in acidic electrolytes.

Author Contributions: X.G.: conceptualization, data curation, investigation, writing—original draft, writing—review and editing; H.D.: conceptualization, data curation, investigation, writing—original draft, writing—review and editing; Q.D.: data curation, writing—original draft; Q.Z.: data curation; S.Q.: funding acquisition, resources, project administration, supervision, validation; X.L.: funding acquisition, resources, project administration, supervision, validation. All authors have read and agreed to the published version of the manuscript.

Funding: This research was funded by Natural Science Foundation of Guangdong Province (2018A-030310301), Guangzhou Basic and Applied Basic Research Project in China (202102020134; 202102020690) and Youth Innovation Talents Project of Guangdong Universities (natural science) in China (2019KQNCX098).

Data Availability Statement: All data included in this study are available upon the permission from the publishers.

Conflicts of Interest: The authors declare no conflict of interest.

References

1. Hua, W.; Sun, H.-H.; Xu, F.; Wang, J.-G. A review and perspective on molybdenum-based electrocatalysts for hydrogen evolution reaction. *Rare Met.* **2020**, *39*, 335–351. [[CrossRef](#)]
2. Weng, C.C.; Ren, J.-T.; Yuan, Z.-Y. Transition Metal Phosphide-Based Materials for Efficient Electrochemical Hydrogen Evolution: A Critical Review. *ChemSusChem* **2020**, *13*, 3357–3375. [[CrossRef](#)] [[PubMed](#)]
3. Niu, S.; Cai, J.; Wang, G. Two-dimensional MoS₂ for hydrogen evolution reaction catalysis: The electronic structure regulation. *Nano Res.* **2021**, *14*, 1985–2002. [[CrossRef](#)]
4. Liu, Y.; Huo, J.; Guo, J.; Lu, L.; Shen, Z.; Chen, W.; Liu, C.; Liu, H. Hierarchical Porous Molybdenum Carbide Based Nanomaterials for Electrocatalytic Hydrogen Production. *Front. Chem.* **2020**, *8*, 426. [[CrossRef](#)] [[PubMed](#)]
5. Zhang, X.; Jia, F.; Song, S. Recent advances in structural engineering of molybdenum disulfide for electrocatalytic hydrogen evolution reaction. *Chem. Eng. J.* **2021**, *405*, 127013. [[CrossRef](#)]
6. Xiong, B.; Chen, L.; Shi, J. Anion-Containing Noble-Metal-Free Bifunctional Electrocatalysts for Overall Water Splitting. *ACS Catal.* **2018**, *8*, 3688–3707. [[CrossRef](#)]
7. McKone, J.R.; Marinescu, S.C.; Brunschwig, B.S.; Winkler, J.R.; Gray, H.B. Earth-abundant hydrogen evolution electrocatalysts. *Chem. Sci.* **2014**, *5*, 865–878. [[CrossRef](#)]
8. Theerthagiri, J.; Senthil, R.A.; Madhavan, J.; Maiyalagan, T. Review on recent progress in non platinum counter electrode materials for dye-sensitized solar cells. *ChemElectroChem* **2015**, *2*, 928–945. [[CrossRef](#)]
9. Jamesh, M.; Kuang, Y.; Sun, X. Constructing Earth-abundant 3D Nanoarrays for Efficient Overall Water Splitting—A Review. *ChemCatChem* **2019**, *11*, 1550–1575. [[CrossRef](#)]
10. Zou, X.; Zhang, Y. Noble metal-free hydrogen evolution catalysts for water splitting. *Chem. Soc. Rev.* **2015**, *44*, 5148–5180. [[CrossRef](#)]
11. Cao, B.; Veith, G.M.; Diaz, R.E.; Liu, J.; Stach, E.A.; Adzic, R.R.; Khalifah, P.G. Cobalt molybdenum oxynitrides: Synthesis, structural characterization, and catalytic activity for the oxygen reduction reaction. *Angew. Chem. Int. Ed.* **2013**, *52*, 10753–10757. [[CrossRef](#)] [[PubMed](#)]
12. Yu, M.; Zhao, S.; Feng, H.; Hu, L.; Zhang, X.; Zeng, Y.; Tong, Y.; Lu, X. Engineering Thin MoS₂ Nanosheets on TiN Nanorods: Advanced Electrochemical Capacitor Electrode and Hydrogen Evolution Electrocatalyst. *ACS Energy Lett.* **2017**, *2*, 1862–1868. [[CrossRef](#)]

13. Deng, S.; Yang, F.; Zhang, Q.; Zhong, Y.; Zeng, Y.; Lin, S.; Wang, X.; Lu, X.; Wang, C.; Lu, L.; et al. Phase Modulation of (1T-2H)-MoSe₂/TiC-C Shell/Core Arrays via Nitrogen Doping for Highly Efficient Hydrogen Evolution Reaction. *Adv. Mater.* **2018**, *30*, 1802223. [[CrossRef](#)]
14. Deng, S.; Zhong, Y.; Zeng, Y.; Wang, Y.; Yao, Z.; Yang, F.; Lin, S.; Wang, X.; Lu, X.; Xia, X.; et al. Directional Construction of Vertical Nitrogen-Doped 1T-2H MoSe₂/Graphene Shell/Core Nanoflake Arrays for Efficient Hydrogen Evolution Reaction. *Adv. Mater.* **2017**, 1700748. [[CrossRef](#)]
15. Fang, M.; Gao, W.; Dong, G.; Xia, Z.; Yip, S.; Qin, Y.; Qu, Y.; Ho, J.C. Hierarchical NiMo-based 3D electrocatalysts for highly-efficient hydrogen evolution in alkaline conditions. *Nano Energy* **2016**, *27*, 247–254. [[CrossRef](#)]
16. Kibsgaard, J.; Chen, Z.; Reinecke, B.N.; Jaramillo, T.F. Engineering the surface structure of MoS₂ to preferentially expose active edge sites for electrocatalysis. *Nat. Mater.* **2012**, *11*, 963–969. [[CrossRef](#)]
17. Huang, Y.; Gong, Q.; Song, X.; Feng, K.; Nie, K.; Zhao, F.; Wang, Y.; Zeng, M.; Zhong, J.; Li, Y. Mo₂C nanoparticles dispersed on hierarchical carbon microflowers for efficient electrocatalytic hydrogen evolution. *ACS Nano* **2016**, *10*, 11337–11343. [[CrossRef](#)]
18. Tsai, C.; Chan, K.; Abild-Pedersen, F.; Norskov, J.K. Active edge sites in MoSe₂ and WSe₂ catalysts for the hydrogen evolution reaction: A density functional study. *Phys. Chem. Chem. Phys.* **2014**, *16*, 13156–13164. [[CrossRef](#)]
19. Xiao, P.; Sk, M.A.; Thia, L.; Ge, X.; Lim, R.J.; Wang, J.Y.; Lim, K.H.; Wang, X. Molybdenum phosphide as an efficient electrocatalyst for the hydrogen evolution reaction. *Energy Environ. Sci.* **2014**, *7*, 2624–2629. [[CrossRef](#)]
20. Park, H.; Zhang, Y.; Scheifers, J.P.; Jothi, P.R.; Encinas, A.; Fokwa, B.P.T. Graphene- and phosphorene-like boron layers with contrasting activities in highly active Mo₂B₄ for hydrogen evolution. *J. Am. Chem. Soc.* **2017**, *139*, 12915–12918. [[CrossRef](#)]
21. Chen, W.F.; Sasaki, K.; Ma, C.; Frenkel, A.I.; Marinkovic, N.; Muckerman, J.T.; Zhu, Y.; Adzic, R.R. Hydrogen-evolution catalysts based on non-noble metal nickel-molybdenum nitride nanosheets. *Angew. Chem. Int. Ed.* **2012**, *51*, 6131–6135. [[CrossRef](#)] [[PubMed](#)]
22. Xie, X.; Yu, R.; Xue, N.; Bin Yousaf, A.; Du, H.; Liang, K.; Jiang, N.; Xu, A.W. P doped molybdenum dioxide on Mo foil with high electrocatalytic activity for the hydrogen evolution reaction. *J. Mater. Chem. A* **2016**, *4*, 1647–1652. [[CrossRef](#)]
23. Wang, Y.; Kong, B.; Zhao, D.; Wang, H.; Selomulya, C. Strategies for developing transition metal phosphides as heterogeneous electrocatalysts for water splitting. *Nano Today* **2017**, *15*, 26–55. [[CrossRef](#)]
24. Yan, Y.; Ge, X.; Liu, Z.; Wang, J.Y.; Lee, J.M.; Wang, X. Facile synthesis of low crystalline MoS₂ nanosheet-coated CNTs for enhanced hydrogen evolution reaction. *Nanoscale* **2013**, *5*, 7768–7771. [[CrossRef](#)]
25. Bian, X.; Zhu, J.; Liao, L.; Scanlon, M.D.; Ge, P.; Ji, C.; Girault, H.H.; Liu, B. Nanocomposite of MoS₂ on ordered mesoporous carbon nanospheres: A highly active catalyst for electrochemical hydrogen evolution. *Electrochim. Commun.* **2012**, *22*, 128–132. [[CrossRef](#)]
26. Zhao, G.; Wang, X.; Wang, S.; Rui, K.; Chen, Y.; Yu, H.; Ma, J.; Dou, S.X.; Sun, W. Heteroatom-doped MoSe₂ nanosheets with enhanced hydrogen evolution kinetics for alkaline water splitting. *Chem. Asian J.* **2019**, *14*, 301–306. [[CrossRef](#)]
27. Zhao, G.; Li, P.; Rui, K.; Chen, Y.; Dou, S.X.; Sun, W. CoSe₂/MoSe₂ heterostructures with enriched water adsorption/dissociation sites towards enhanced alkaline hydrogen evolution reaction. *Chem. Eur. J.* **2018**, *24*, 11158–11165. [[CrossRef](#)]
28. Shinagawa, T.; Garcia-Esparza, A.T.; Takanebe, K. Insight on Tafel slopes from a microkinetic analysis of aqueous electrocatalysis for energy conversion. *Sci. Rep.* **2015**, *5*, 13801. [[CrossRef](#)]
29. Du, H.; Kong, R.M.; Guo, X.; Qu, F.; Li, J. Recent progress in transition metal phosphides with enhanced electrocatalysis for hydrogen evolution. *Nanoscale* **2018**, *10*, 21617–21624. [[CrossRef](#)]
30. Zhao, X.; Sun, W.; Geng, D.; Fu, W.; Dan, J.; Xie, Y.; Kent, P.R.C.; Zhou, W.; Pennycook, S.J.; Loh, K.P. Edge segregated polymorphism in 2D molybdenum carbide. *Adv. Mater.* **2019**, *31*, 1808343. [[CrossRef](#)]
31. Brown, D.E.; Mahmood, M.N.; Man, M.C.M.; Turner, A.K. Preparation and characterization of low overvoltage transition metal alloy electrocatalysts for hydrogen evolution in alkaline solutions. *Electrochim. Acta* **1984**, *29*, 1551–1556. [[CrossRef](#)]
32. Zhang, J.; Wang, T.; Liu, P.; Liao, Z.; Liu, S.; Zhuang, X.; Chen, M.; Zschech, E.; Feng, X. Efficient hydrogen production on MoNi₄ electrocatalysts with fast water dissociation kinetics. *Nat. Commun.* **2017**, *8*, 15437. [[CrossRef](#)]
33. Li, X.; Jiang, Y.; Jia, L.; Wang, C. MoO₂ nanoparticles on reduced graphene oxide/polyimide-carbon nanotube film as efficient hydrogen evolution electrocatalyst. *J. Power Sources* **2016**, *304*, 146–154. [[CrossRef](#)]
34. Wu, L.; Wang, X.; Sun, Y.; Liu, Y.; Li, J. Flawed MoO₂ belts transformed from MoO₃ on a graphene template for the hydrogen evolution reaction. *Nanoscale* **2015**, *7*, 7040–7044. [[CrossRef](#)] [[PubMed](#)]
35. Jin, Y.; Shen, P.K. Nanoflower-like metallic conductive MoO₂ as a high-performance non-precious metal electrocatalyst for the hydrogen evolution reaction. *J. Mater. Chem. A* **2015**, *3*, 20080–20085. [[CrossRef](#)]
36. Jin, Y.; Wang, H.; Li, J.; Yue, X.; Han, Y.; Shen, P.K.; Cui, Y. Porous MoO₂ nanosheets as non-noble bifunctional electrocatalysts for overall water splitting. *Adv. Mater.* **2016**, *28*, 3785–3790. [[CrossRef](#)] [[PubMed](#)]
37. Ren, B.; Li, D.; Jin, Q.; Cui, H.; Wang, C. Integrated 3D self-supported Ni decorated MoO₂ nanowires as highly efficient electrocatalysts for ultra-highly stable and large-current-density hydrogen evolution. *J. Mater. Chem. A* **2017**, *5*, 24453–24461. [[CrossRef](#)]
38. Hinnemann, B.; Moses, P.G.; Bonde, J.; Jørgensen, K.P.; Nielsen, J.H.; Hørch, S.; Chorkendorff, I.; Nørskov, J.K. Biomimetic hydrogen evolution: MoS₂ nanoparticles as catalyst for hydrogen evolution. *J. Am. Chem. Soc.* **2005**, *127*, 5308–5309. [[CrossRef](#)]
39. Han, N.; Liu, P.; Jiang, J.; Ai, L.; Shao, Z.; Liu, S. Recent advances in nanostructured metal nitrides for water splitting. *J. Mater. Chem. A* **2018**, *6*, 19912–19933. [[CrossRef](#)]

40. Yuan, N.; Jiang, Q.; Li, J.; Tang, J. A review on non-noble metal based electrocatalysis for the oxygen evolution reaction. *Arab. J. Chem.* **2020**, *13*, 4294–4309. [[CrossRef](#)]
41. Hulliger, F. Crystal chemistry of the chalcogenides and pnictides of the transition elements. *Struct. Bond.* **1968**, *4*, 83–229.
42. Callejas, J.F.; Read, C.G.; Roske, C.W.; Lewis, N.S.; Schaak, R.E. Synthesis, Characterization, and Properties of Metal Phosphide Catalysts for the Hydrogen-Evolution Reaction. *Chem. Mater.* **2016**, *28*, 6017–6044. [[CrossRef](#)]
43. Ryoo, R. Birth of a class of nanomaterial. *Nature* **2019**, *575*, 40–41. [[CrossRef](#)]
44. Wan, C.; Regmi, Y.N.; Leonard, B.M. Multiple phases of molybdenum carbide as electrocatalysts for the hydrogen evolution reaction. *Angew. Chem. Int. Ed.* **2014**, *53*, 6407–6410. [[CrossRef](#)]
45. Park, H.; Encinas, A.; Scheifers, J.P.; Zhang, Y.; Fokwa, B.P.T. Boron-dependency of molybdenum boride electrocatalysts for the hydrogen evolution reaction. *Angew. Chem. Int. Ed.* **2017**, *56*, 5575–5578. [[CrossRef](#)] [[PubMed](#)]
46. Vrabel, H.; Hu, X. Molybdenum boride and carbide catalyze hydrogen evolution in both acidic and basic solutions. *Angew. Chem. Int. Ed.* **2012**, *51*, 12703–12706. [[CrossRef](#)] [[PubMed](#)]
47. Zhu, H.; Du, M.; Zhang, M.; Zou, M.; Yang, T.; Fu, Y.; Yao, J. The design and construction of 3D rose-petal-shaped MoS₂ hierarchical nanostructures with structure-sensitive properties. *J. Mater. Chem. A* **2014**, *2*, 7680–7685. [[CrossRef](#)]
48. Zheng, X.; Xu, J.; Yan, K.; Wang, H.; Wang, Z.; Yang, S. Space-confined growth of MoS₂ nanosheets within graphite: The layered hybrid of MoS₂ and graphene as an active catalyst for hydrogen evolution reaction. *Chem. Mater.* **2014**, *26*, 2344–2353. [[CrossRef](#)]
49. Ma, C.B.; Qi, X.; Chen, B.; Bao, S.; Yin, Z.; Wu, X.J.; Luo, Z.; Wei, J.; Zhang, H.L.; Zhang, H. MoS₂ nanoflower-decorated reduced graphene oxide paper for high-performance hydrogen evolution reaction. *Nanoscale* **2014**, *6*, 5624–5629. [[CrossRef](#)] [[PubMed](#)]
50. Yang, J.; Zhang, F.; Wang, X.; He, D.; Wu, G.; Yang, Q.; Hong, X.; Wu, Y.; Li, Y. Porous molybdenum phosphide nano-octahedrons derived from confined phosphorization in UIO-66 for efficient hydrogen evolution. *Angew. Chem. Int. Ed.* **2016**, *55*, 12854–12858. [[CrossRef](#)]
51. Bonde, J.; Moses, P.G.; Jaramillo, T.F.; Nørskov, J.K.; Chorkendorff, I. Hydrogen evolution on nano-particulate transition metal sulfide. *Faraday Discuss.* **2009**, *140*, 219–231. [[CrossRef](#)]
52. Sun, X.; Dai, J.; Guo, Y.; Wu, C.; Hu, F.; Zhao, J.; Zeng, X.; Xie, Y. Semimetallic molybdenum disulfide ultrathin nanosheets as an efficient electrocatalyst for hydrogen evolution. *Nanoscale* **2014**, *6*, 8359–8367. [[CrossRef](#)] [[PubMed](#)]
53. Zhang, J.; Wang, T.; Liu, P.; Liu, S.; Dong, R.; Zhuang, X.; Chen, M.; Feng, X. Engineering water dissociation sites in MoS₂ nanosheets for accelerated electrocatalytic hydrogen production. *Energy Environ. Sci.* **2016**, *9*, 2789–2793. [[CrossRef](#)]
54. Xu, C.; Peng, S.; Tan, C.; Ang, H.; Tan, H.; Zhang, H.; Yan, Q. Ultrathin S-doped MoSe₂ nanosheets for efficient hydrogen evolution. *J. Mater. Chem. A* **2014**, *2*, 5597–5601. [[CrossRef](#)]
55. Zhang, J.; Wang, T.; Pohl, D.; Rellinghaus, B.; Dong, R.; Liu, S.; Zhuang, X.; Feng, X. Interface engineering of MoS₂/Ni₃S₂ heterostructures for highly enhanced electrochemical overall-water-splitting activity. *Angew. Chem. Int. Ed.* **2016**, *55*, 6702–6707. [[CrossRef](#)]
56. Wang, D.; Liu, T.; Wang, J.; Wu, Z. N, P (S) Co-doped Mo₂C/C hybrid electrocatalysts for improved hydrogen generation. *Carbon* **2018**, *139*, 845–852. [[CrossRef](#)]
57. Lan, K.; Gong, L.; Yang, M.; Huang, X.; Jiang, P.; Wang, K.; Ma, L.; Li, R. Nitrogen and phosphorus dual-doping carbon shells encapsulating ultrafine Mo₂C particles as electrocatalyst for hydrogen evolution. *J. Colloid Interfaces Sci.* **2019**, *553*, 148–155. [[CrossRef](#)]
58. Liu, X.; Zhang, L.; Lan, X.; Hu, X. Paragenesis of Mo₂C nanocrystals in mesoporous carbon nanofibers for electrocatalytic hydrogen evolution. *Electrochim. Acta* **2018**, *274*, 23–30. [[CrossRef](#)]
59. Zhang, L.; Li, S.; Tan, H.; Khan, S.U.; Ma, Y.; Zang, H.; Wang, Y.; Li, Y. MoP/Mo₂C@C: A New Combination of Electrocatalysts for Highly Efficient Hydrogen Evolution over the Entire pH Range. *ACS Appl. Mater. Interfaces* **2017**, *9*, 16270–16279. [[CrossRef](#)] [[PubMed](#)]
60. Chen, N.; Mo, Q.; He, L.; Huang, X.; Yang, L.; Zeng, J.; Gao, Q. Heterostructured MoC-MoP/N-doped carbon nanofibers as efficient electrocatalysts for hydrogen evolution reaction. *Electrochim. Acta* **2019**, *299*, 708–716. [[CrossRef](#)]
61. Fan, X.; Liu, Y.; Peng, Z.; Zhang, Z.; Zhou, H.; Zhang, X.; Jakobson, B.I.; Goddard, W.A., III; Guo, X.; Hauge, R.H.; et al. Atomic H-Induced Mo₂C Hybrid as an Active and Stable Bifunctional Electrocatalyst. *ACS Nano* **2017**, *11*, 384–394. [[CrossRef](#)]
62. An, K.; Xu, X. Mo₂C based electrocatalyst with nitrogen doped three-dimensional mesoporous carbon as matrix, synthesis and HER activity study. *Electrochim. Acta* **2019**, *293*, 348–355. [[CrossRef](#)]
63. Qamar, M.; Adam, A.; Merzougui, B.; Helal, A.; Abdulhamid, O.; Siddiqui, M.N. Metal-organic framework-guided growth of Mo₂C embedded in mesoporous carbon as a highperformance and stable electrocatalyst for the hydrogen evolution reaction. *J. Mater. Chem. A* **2016**, *4*, 16225–16232. [[CrossRef](#)]
64. Xu, B.; Sun, Y.; Chen, Z.; Zhao, S.; Yang, X.; Zhang, H.; Li, C. Facile and large-scale preparation of Co/Ni-MoO₂ composite as high-performance electrocatalyst for hydrogen evolution reaction. *Int. J. Hydrogen Energy* **2018**, *43*, 20721–20726. [[CrossRef](#)]
65. Jian, C.; Hong, W.; Cai, Q.; Li, J.; Liu, W. Surface electron state engineering enhanced hydrogen evolution of hierarchical molybdenum disulfide in acidic and alkaline media. *Appl. Catal. B Environ.* **2020**, *266*, 118649. [[CrossRef](#)]
66. Wang, B.; Huang, H.; Huang, M.; Yan, P.; Isimjan, T.T.; Yang, X. Electron-transfer enhanced MoO₂-Ni heterostructures as a highly efficient pH-universal catalyst for hydrogen evolution. *Sci. China Chem.* **2020**, *63*, 841–849. [[CrossRef](#)]
67. Jiao, Y.; Yan, H.; Wang, R.; Wang, X.; Zhang, X.; Wu, A.; Tian, C.; Jiang, B.; Fu, H. Porous Plate-like MoP Assembly as an Efficient pH-Universal Hydrogen Evolution Electrocatalyst. *ACS Appl. Mater. Interfaces* **2020**, *12*, 49596–49606. [[CrossRef](#)]

68. Zhao, D.; Sun, K.; Cheong, W.-C.; Zheng, L.; Zhang, C.; Liu, S.; Cao, X.; Wu, K.; Pan, Y.; Zhuang, Z.; et al. Synergistically Interactive Pyridinic-N–MoP Sites: Identified Active Centers for Enhanced Hydrogen Evolution in Alkaline Solution. *Angew. Chem. Int. Ed.* **2020**, *59*, 8982–8990. [[CrossRef](#)]
69. Zhao, H.; Li, Z.; Dai, X.; Cui, M.; Nie, F.; Zhang, X.; Ren, Z.; Yang, Z.; Gan, Y.; Yin, X.; et al. Heterostructured CoP/MoO₂ on Mo foil as high-efficiency electrocatalysts for the hydrogen evolution reaction in both acidic and alkaline media. *J. Mater. Chem. A* **2020**, *8*, 6732–6739. [[CrossRef](#)]
70. Huang, Y.; Xie, X.; Zhang, Y.; Ding, J.; Liu, L.; Fang, Y.; Lv, H.; Liu, Y.; Cai, Q. Hard template strategy for the synthesis of porous MoS₂/MoO₂ hybrid electrocatalyst for hydrogen evolution reaction. *Appl. Surf. Sci.* **2020**, *520*, 146340. [[CrossRef](#)]
71. Li, J.; Zhang, S.; Sha, J.; Wang, H.; Liu, M.; Kong, L.; Liu, G. Confined Molybdenum Phosphide in P-Doped Porous Carbon as Efficient Electrocatalysts for Hydrogen Evolution. *ACS Appl. Mater. Interfaces* **2018**, *10*, 17140–17146. [[CrossRef](#)]
72. Hu, Z.; Huang, J.; Luo, Y.; Liu, M.; Li, X.; Yan, M.; Ye, Z.; Chen, Z.; Feng, Z.; Huang, S. Wrinkled Ni-doped Mo₂C coating on carbon fiber paper: An advanced electrocatalyst prepared by molten-salt method for hydrogen evolution reaction. *Electrochim. Acta* **2019**, *319*, 293–301. [[CrossRef](#)]
73. Zhang, Y.; Zang, J.; Han, C.; Jia, S.; Tian, P.; Gao, H.; Wang, Y. Molybdenum oxide and molybdenum carbide coated carbon black as an electrocatalyst for hydrogen evolution reaction in acidic media. *Int. J. Hydrogen Energy* **2017**, *42*, 26985–26994. [[CrossRef](#)]
74. Song, Y.; Ren, J.; Yuan, G.; Yao, Y.; Liu, X.; Yuan, Z. Facile synthesis of Mo₂C nanoparticles on N-doped carbon nanotubes with enhanced electrocatalytic activity for hydrogen evolution and oxygen reduction reactions. *J. Energy Chem.* **2019**, *38*, 68–77. [[CrossRef](#)]
75. Anjum, M.A.R.; Lee, J.S. Sulfur and Nitrogen Dual-Doped Molybdenum Phosphide Nanocrystallites as an Active and Stable Hydrogen Evolution Reaction Electrocatalyst in Acidic and Alkaline Media. *ACS Catal.* **2017**, *7*, 3030–3038. [[CrossRef](#)]
76. Wang, M.; Jian, K.; Lv, Z.; Li, D.; Fan, G.; Zhang, R.; Dang, J. MoS₂/Co₉S₈/MoC heterostructure connected by carbon nanotubes as electrocatalyst for efficient hydrogen evolution reaction. *J. Mater. Sci. Technol.* **2021**, *79*, 29–34. [[CrossRef](#)]
77. Wang, D.; Wang, J.; Luo, X.; Wu, Z.; Ye, L. In Situ Preparation of Mo₂C Nanoparticles Embedded in Ketjenblack Carbon as Highly Efficient Electrocatalysts for Hydrogen Evolution. *ACS Sustain. Chem. Eng.* **2018**, *6*, 983–990. [[CrossRef](#)]
78. Xing, J.; Li, Y.; Guo, S.; Jin, T.; Li, H.; Wang, Y.; Jiao, L. Molybdenum carbide in-situ embedded into carbon nanosheets as efficient bifunctional electrocatalysts for overall water splitting. *Electrochim. Acta* **2019**, *298*, 305–312. [[CrossRef](#)]
79. Zhang, L.; Yang, Y.; Ziaee, M.A.; Lu, K.; Wang, R. Nanohybrid of Carbon Quantum Dots/Molybdenum Phosphide Nanoparticle for Efficient Electrochemical Hydrogen Evolution in Alkaline Medium. *ACS Appl. Mater. Interfaces* **2018**, *10*, 9460–9467. [[CrossRef](#)] [[PubMed](#)]
80. Adam, A.; Suliman, M.H.; Dafalla, H.; Al-Arfaj, A.R.; Siddiqui, M.N.; Qamar, M. Rationally dispersed molybdenum phosphide on carbon nanotubes for the hydrogen evolution reaction. *ACS Sustain. Chem. Eng.* **2018**, *6*, 11414–11423. [[CrossRef](#)]
81. Adam, A.; Suliman, M.H.; Awwad, M.; Siddiqui, M.N.; Yamani, Z.H.; Qamar, M. Controlled growth of small and uniformly dispersed Mo₂C on carbon nanotubes as high performance electrocatalyst for the hydrogen evolution reaction. *Int. J. Hydrogen Energy* **2019**, *44*, 11797–11807. [[CrossRef](#)]
82. Lin, H.; Shi, Z.; He, S.; Yu, X.; Wang, S.; Gao, Q.; Tang, Y. Heteronanowires of MoC–Mo₂C as efficient electrocatalysts for hydrogen evolution reaction. *Chem. Sci.* **2016**, *7*, 3399–3405. [[CrossRef](#)]
83. Li, J.S.; Wang, Y.; Liu, C.H.; Li, S.L.; Wang, Y.G.; Dong, L.Z.; Dai, Z.H.; Li, Y.F.; Lan, Y.Q. Coupled molybdenum carbide and reduced graphene oxide electrocatalysts for efficient hydrogen evolution. *Nat. Commun.* **2016**, *7*, 11204. [[CrossRef](#)] [[PubMed](#)]
84. Wu, Z.; Hu, B.; Wu, P.; Liang, H.; Yu, Z.; Lin, Y.; Zheng, Y.; Li, Z.; Yu, S. Mo₂C nanoparticles embedded within bacterial cellulose-derived 3D N-doped carbon nanofiber networks for efficient hydrogen evolution. *NPG Asia Mater.* **2016**, *8*, e288. [[CrossRef](#)]
85. Wang, Y.; Hu, A. Carbon Quantum Dots: Synthesis, Properties and Applications. *J. Mater. Chem. C* **2014**, *2*, 6921–6939. [[CrossRef](#)]
86. Yan, H.; Jiao, Y.; Wu, A.; Tian, C.; Zhang, X.; Wang, L.; Ren, Z.; Fu, H. Cluster-Like Molybdenum Phosphide Anchored on Reduced Graphene Oxide for Efficient Hydrogen Evolution over a Broad pH Range. *Chem. Commun.* **2016**, *52*, 9530–9533. [[CrossRef](#)]
87. Tang, Y.-J.; Wang, Y.; Wang, X.-L.; Li, S.-L.; Huang, W.; Dong, L.-Z.; Liu, C.-H.; Li, Y.-F.; Lan, Y.-Q. Molybdenum Disulfide/Nitrogen-Doped Reduced Graphene Oxide Nanocomposite with Enlarged Interlayer Spacing for Electrocatalytic Hydrogen Evolution. *Adv. Energy Mater.* **2016**, *6*, 1600116. [[CrossRef](#)]
88. Kang, Q.; Li, M.; Wang, Z.; Lu, Q.; Gao, F. Agaric-derived N-doped carbon nanorod arrays@nanosheet networks coupled with molybdenum carbide nanoparticles as highly efficient pH-universal hydrogen evolution electrocatalysts. *Nanoscale* **2020**, *12*, 5159–5169. [[CrossRef](#)] [[PubMed](#)]
89. Poorahong, S.; Harding, D.J.; Siaj, M. Hollow molybdenum oxide-graphene oxide spheres as a binder-free electrocatalyst membrane with enhanced hydrogen evolution efficiency. *Mater. Lett.* **2020**, *272*, 127872. [[CrossRef](#)]
90. Li, Y.; Wang, H.; Xie, L.; Liang, Y.; Hong, G.; Dai, H. MoS₂ Nanoparticles Grown on Graphene: An Advanced Catalyst for the Hydrogen Evolution Reaction. *J. Am. Chem. Soc.* **2011**, *133*, 7296–7299. [[CrossRef](#)] [[PubMed](#)]
91. Xu, C.; Xu, B.; Gu, Y.; Xiong, Z.; Sun, J.; Zhao, X.S. Graphene-Based Electrodes for Electrochemical Energy Storage. *Energy Environ. Sci.* **2013**, *6*, 1388–1414. [[CrossRef](#)]
92. Wang, Y.; Zhu, S.; Tsubaki, N.; Wu, M. Highly Dispersed Mo₂C Anchored on N,P-Codoped Graphene as Efficient Electrocatalyst for Hydrogen Evolution Reaction. *ChemCatChem* **2018**, *10*, 2300–2304. [[CrossRef](#)]

93. Li, X.; Ci, S.; Jia, J.; Wen, Z. Graphene Loading Molybdenum Carbide/Oxide Hybrids as Advanced Electrocatalysts for hydrogen evolution reaction. *Int. J. Hydrogen Energy* **2016**, *41*, 21246–21250. [[CrossRef](#)]
94. Wu, Z.; Wang, J.; Zhu, J.; Guo, J.; Xiao, W.; Xuan, C.; Lei, W.; Wang, D. Highly efficient and stable MoP-rGO nanoparticles as electrocatalysts for hydrogen evolution. *Electrochim. Acta* **2017**, *232*, 254–261. [[CrossRef](#)]
95. Zhang, Y.; Yang, J.; Dong, Q.; Geng, H.; Zheng, Y.; Liu, Y.; Wang, W.; Li, C.; Dong, X. Highly Dispersive MoP Nanoparticles Anchored on Reduced Graphene Oxide Nanosheets for an Efficient Hydrogen Evolution Reaction Electrocatalyst. *ACS Appl. Mater. Interfaces* **2018**, *10*, 26258–26263. [[CrossRef](#)] [[PubMed](#)]
96. Guo, P.; Song, H.; Chen, X. Hollow graphene oxide spheres self-assembled by W/O emulsion. *J. Mater. Chem.* **2010**, *20*, 4867–4874. [[CrossRef](#)]
97. Chang, J.; Jin, M.; Yao, F.; Kim, T.H.; Le, V.T.; Yue, H.; Gunes, F.; Li, B.; Ghosh, A.; Xie, S.; et al. Asymmetric Supercapacitors Based on Graphene/MnO₂ Nanospheres and Graphene/MoO₃ Nanosheets with High Energy Density. *Adv. Funct. Mater.* **2013**, *23*, 5074–5083. [[CrossRef](#)]
98. Wang, H.; Zhang, Q.; Yao, H.; Liang, Z.; Lee, H.-W.; Hsu, P.-C.; Zheng, G.; Cui, Y. High Electrochemical Selectivity of Edge versus Terrace Sites in Two-Dimensional Layered MoS₂ Materials. *Nano Lett.* **2014**, *14*, 7138–7144. [[CrossRef](#)] [[PubMed](#)]
99. Youn, D.H.; Han, S.; Kim, J.Y.; Kim, J.Y.; Park, H.; Choi, S.H.; Lee, J.S. Highly Active and Stable Hydrogen Evolution Electrocatalysts Based on Molybdenum Compounds on Carbon Nanotube–Graphene Hybrid Support. *ACS Nano* **2014**, *8*, 5164–5173. [[CrossRef](#)]
100. Sing, K.S.W.; Everett, D.H.; Haul, R.A.; Moscou, L.; Pierotti, R.A.; Rouquérol, J.; Siemieniewska, T. Reporting physisorption data for gas/solid systems with special reference to the determination of surface area and porosity. *Pure Appl. Chem.* **1985**, *57*, 603–619. [[CrossRef](#)]
101. Chi, J.Q.; Lin, J.H.; Qin, J.F.; Dong, B.; Yan, K.L.; Liu, Z.Z.; Zhang, X.Y.; Chai, Y.M.; Liu, C.G. A triple synergistic effect from pitaya-like MoNi_x-MoC_x hybrids encapsulated in N-doped C nanospheres for efficient hydrogen evolution. *Sustain. Energy Fuels* **2018**, *2*, 1610–1620. [[CrossRef](#)]
102. Li, Z.; Zou, K.; Zhang, X.; Han, T.; Yang, Y. Hierarchically flower-like N-doped porous carbon materials derived from an explosive 3-Fold interpenetrating diamondoid copper metal-organic framework for a supercapacitor. *Inorg. Chem.* **2016**, *55*, 6552–6562. [[CrossRef](#)] [[PubMed](#)]
103. An, K.; Xu, X.; Liu, X. Mo₂C-Based Electrocatalyst with Biomass-Derived Sulfur and Nitrogen Co-Doped Carbon as a Matrix for Hydrogen Evolution and Organic Pollutant Removal. *ACS Sustain. Chem. Eng.* **2018**, *6*, 1446–1455. [[CrossRef](#)]
104. Liu, J.; Zhang, F.; Zou, X.; Yu, G.; Zhao, N.; Fan, F.; Zhu, G. Environmentally friendly synthesis of highly hydrophobic and stable MIL-53 MOF nanomaterials. *Chem. Commun.* **2013**, *49*, 7430–7432. [[CrossRef](#)]
105. Roberts, A.D.; Wang, S.; Li, X.; Zhang, H. Hierarchical porous nitrogen-rich carbon monoliths via ice-templating: High capacity and high-rate performance as lithium-ion battery anode materials. *J. Mater. Chem. A* **2014**, *2*, 17787–17796. [[CrossRef](#)]
106. Giesche, H. Mercury Porosimetry: A General (Practical) Overview. *Part. Part. Syst. Charact.* **2006**, *23*, 9–19. [[CrossRef](#)]
107. Fletcher, S. Physical electrochemistry. Fundamentals, techniques, and applications by Eliezer Gileadi. *J. Solid State Electrochem.* **2012**, *16*, 1301. [[CrossRef](#)]
108. Yang, X.J.; Feng, X.J.; Tan, H.Q.; Zang, H.Y.; Wang, X.L.; Wang, Y.H.; Wang, E.B.; Li, Y.G. N-doped Graphene-Coated Molybdenum Carbide Nanoparticles as High Efficient Electrocatalyst for Hydrogen Evolution Reaction. *J. Mater. Chem. A* **2016**, *4*, 3947–3954. [[CrossRef](#)]
109. Zheng, Y.; Jiao, Y.; Jaroniec, M.; Qiao, S.Z. Advancing the Electrochemistry of the Hydrogen-Evolution Reaction through Combining Experiment and Theory. *Angew. Chem. Int. Ed.* **2015**, *54*, 52–65. [[CrossRef](#)]
110. Ma, T.Y.; Dai, S.; Jaroniec, M.; Qiao, S.Z. Metal–Organic Framework Derived Hybrid Co₃O₄-Carbon Porous Nanowire Arrays as Reversible Oxygen Evolution Electrodes. *J. Am. Chem. Soc.* **2014**, *136*, 13925–13931. [[CrossRef](#)]
111. Yu, F.; Gao, Y.; Liang, Z.; Ma, Y.; Yin, L.; Du, J.; Tan, H.; Wang, Y.; Li, Y. Electrocatalytic performance of ultrasmall Mo₂C affected by different transition metal dopants in hydrogen evolution reaction. *Nanoscale* **2018**, *10*, 6080–6087. [[CrossRef](#)] [[PubMed](#)]
112. Tang, C.; Zhang, H.; Xu, K.; Zhang, Q.; Liu, J.; He, C.; Fan, L.; Asefa, T. Unconventional molybdenum carbide phases with high electrocatalytic activity for hydrogen evolution reaction. *J. Mater. Chem. A* **2019**, *7*, 18030–18038. [[CrossRef](#)]
113. Song, Y.; Yuan, Z. One-pot Synthesis of Mo₂N/NC Catalysts with Enhanced Electrocatalytic Activity for Hydrogen Evolution Reaction. *Electrochim. Acta* **2017**, *246*, 536–543. [[CrossRef](#)]
114. Vancsó, P.; Popov, Z.I.; Pető, J.; Ollár, T.; Dobrik, G.; Pap, J.S.; Hwang, C.; Sorokin, P.B.; Tapasztó, L. Transition Metal Chalcogenide Single Layers as an Active Platform for Single-Atom Catalysis. *ACS Energy Lett.* **2019**, *4*, 1947–1953. [[CrossRef](#)]
115. Chen, J.; Yang, H.; Xu, X.; Su, Z.; Guo, Y.; Wang, Q. Mo₂C based electrocatalyst with filter paper derived N-doped mesoporous carbon as matrix for H₂ production. *Appl. Surf. Sci.* **2018**, *455*, 187–194. [[CrossRef](#)]
116. Kibsgaard, J.; Jaramillo, T.F. Molybdenum Phosphosulfide: An Active, Acid-Stable, Earth-Abundant Catalyst for the Hydrogen Evolution Reaction. *Angew. Chem.* **2014**, *126*, 14661–14665. [[CrossRef](#)]
117. Li, Y.; Cai, L.; Huang, Q.; Liu, J.; Tang, R.; Zhou, W. Highly Efficient Synthesis of Carbon-Based Molybdenum Phosphide Nanoparticles for Electrocatalytic Hydrogen Evolution. *Nanoscale Res. Lett.* **2020**, *15*, 6. [[CrossRef](#)]
118. Lei, Y.; Jia, M.; Guo, P.; Liu, J.; Zhai, J. MoP nanoparticles encapsulated in P-doped carbon as an efficient electrocatalyst for the hydrogen evolution reaction. *Catal. Commun.* **2020**, *140*, 106000. [[CrossRef](#)]

119. Liu, Y.; Gou, J.; Li, X.; Dong, B.; Han, G.; Hu, W.; Shang, X.; Chai, Y.; Liu, Y.; Liu, C. Self-sacrificial template method of $\text{Mo}_3\text{O}_{10}(\text{C}_6\text{H}_8\text{N})_2 \cdot 2\text{H}_2\text{O}$ to fabricate MoS_2 /carbon-doped MoO_2 nanobelts as efficient electrocatalysts for hydrogen evolution reaction. *Electrochim. Acta* **2016**, *216*, 397–404. [[CrossRef](#)]
120. Wang, S.; Wang, J.; Li, P.; Wu, Z.; Liu, X. N,P-Codoped Carbon Layer Coupled with MoP Nanoparticles as an Efficient Electrocatalyst for Hydrogen Evolution Reaction. *Materials* **2018**, *11*, 1316. [[CrossRef](#)]
121. Jiang, A.; Wang, Z.; Li, Q.; Dong, M. Ionic Liquid-Assisted Synthesis of Hierarchical One-Dimensional MoP/NPC for High-Performance Supercapacitor and Electrocatalysis. *ACS Sustain. Chem. Eng.* **2020**, *8*, 6343–6351. [[CrossRef](#)]
122. Yang, W.; Tian, J.; Hou, L.; Deng, B.; Wang, S.; Li, R.; Yang, F.; Li, Y. Hierarchical MoP Hollow Nanospheres Anchored on a N,P,S-Doped Porous Carbon Matrix as Efficient Electrocatalysts for the Hydrogen Evolution Reaction. *ChemSusChem* **2019**, *12*, 4662–4670. [[CrossRef](#)]
123. Jia, J.; Xiong, T.; Zhao, L.; Wang, F.; Liu, H.; Hu, R.; Zhou, J.; Zhou, W.; Chen, S. Ultrathin N-Doped Mo_2C Nanosheets with Exposed Active Sites as Efficient Electrocatalyst for Hydrogen Evolution Reactions. *ACS Nano* **2017**, *11*, 12509–12518. [[CrossRef](#)] [[PubMed](#)]
124. Huang, Y.; Song, X.; Deng, J.; Zha, C.; Huang, W.; Wu, Y.; Li, Y. Ultra-dispersed molybdenum phosphide and phosphosulfide nanoparticles on hierarchical carbonaceous scaffolds for hydrogen evolution electrocatalysis. *Appl. Catal. B Environ.* **2019**, *245*, 656–661. [[CrossRef](#)]
125. Lu, C.; Tranca, D.; Zhang, J.; Hernandez, F.R.; Su, Y.; Zhuang, X.; Zhang, F.; Seifert, G.; Feng, X. Molybdenum Carbide-Embedded Nitrogen-Doped Porous Carbon Nanosheets as Electrocatalysts for Water Splitting in Alkaline Media. *ACS Nano* **2017**, *11*, 3933–3942. [[CrossRef](#)] [[PubMed](#)]
126. Tang, C.; Titirici, M.-M.; Zhang, Q. A review of nanocarbons in energy electrocatalysis: Multifunctional substrates and highly active sites. *J. Energy Chem.* **2017**, *26*, 1077–1093. [[CrossRef](#)]
127. Luo, X.H.; Zhou, Q.L.; Du, S.H.; Li, J.; Zhong, J.W.; Deng, X.L.; Liu, Y.L. Porous Co_9S_8 /Nitrogen, sulfur-doped carbon@ Mo_2C dual catalyst for efficient water splitting. *ACS Appl. Mater. Interfaces* **2018**, *10*, 22291–22302. [[CrossRef](#)]
128. Ma, R.; Zhou, Y.; Chen, Y.; Li, P.; Liu, Q.; Wang, J. Ultrafine Molybdenum Carbide Nanoparticles Compositing with Carbon as a Highly Active Hydrogen-Evolution Electrocatalyst. *Angew. Chem. Int. Ed.* **2015**, *54*, 14723–14727. [[CrossRef](#)]
129. Subbaraman, R.; Tripkovic, D.; Strmcnik, D.; Chang, K.; Uchimura, M.; Paulikas, A.P.; Stamenkovic, V.; Markovic, N.M. Enhancing Hydrogen Evolution Activity in Water Splitting by Tailoring Li^+ -Ni(OH) $_2$ -Pt Interfaces. *Science* **2011**, *334*, 1256–1260. [[CrossRef](#)]
130. Chen, P.; Zhou, T.; Xing, L.; Xu, K.; Tong, Y.; Xie, H.; Zhang, L.; Yan, W.; Chu, W.; Wu, C.; et al. Atomically Dispersed Iron–Nitrogen Species as Electrocatalysts for Bifunctional Oxygen Evolution and Reduction Reactions. *Angew. Chem. Int. Ed.* **2017**, *56*, 610–614. [[CrossRef](#)]
131. Shi, Z.; Nie, K.; Shao, Z.-J.; Gao, B.; Lin, H.; Zhang, H.; Liu, B.; Wang, Y.; Zhang, Y.; Sun, X.; et al. Phosphorus-Mo $_2\text{C}$ @carbon nanowires toward efficient electrochemical hydrogen evolution: Composition, structural and electronic regulation. *Energy Environ. Sci.* **2017**, *10*, 1262–1271. [[CrossRef](#)]
132. Zheng, Y.; Jiao, Y.; Vasileff, A.; Qiao, S.-Z. The Hydrogen Evolution Reaction in Alkaline Solution: From Theory, Single Crystal Models, to Practical Electrocatalysts. *Angew. Chem. Int. Ed.* **2018**, *57*, 7568–7579. [[CrossRef](#)]
133. Li, Y.; Nidamanuri, N.P.; Jiang, A.; Wang, Z.; Li, Q.; Dong, M. In situ construction of tandem nitrogen-doped MoP nanocrystals for high-efficient electrocatalytic hydrogen evolution. *Electrochim. Acta* **2020**, *342*, 136059. [[CrossRef](#)]
134. Li, J.-S.; Tang, Y.-J.; Liu, C.-H.; Li, S.-L.; Li, R.-H.; Dong, L.-Z.; Dai, Z.-H.; Bao, J.-C.; Lan, Y.-Q. Polyoxometalate-Based Metal-Organic Framework-Derived Hybrid Electrocatalysts for Highly Efficient Hydrogen Evolution Reaction. *J. Mater. Chem. A* **2016**, *4*, 1202–1207. [[CrossRef](#)]
135. Yu, J.; Li, W.J.; Zhang, H.S.; Zhou, F.; Li, R.M.; Xu, C.Y.; Zhou, L.M.; Zhong, H.; Wang, J. Metallic FePSe $_3$ nanoparticles anchored on N-doped carbon framework for All-pH hydrogen evolution reaction. *Nano Energy* **2019**, *57*, 222–229. [[CrossRef](#)]
136. Miao, M.; Pan, J.; He, T.; Yan, Y.; Xia, B.Y.; Wang, X. Molybdenum carbide-based electrocatalysts for hydrogen evolution reaction. *Chem. Eur. J.* **2017**, *23*, 10947–10961. [[CrossRef](#)]
137. Xiong, K.; Li, L.; Zhang, L.; Ding, W.; Peng, L.; Wang, Y.; Chen, S.; Tan, S.; Wei, Z. Ni-doped Mo_2C nanowires supported on Ni foam as a binder-free electrode for enhancing the hydrogen evolution performance. *J. Mater. Chem. A* **2015**, *3*, 1863–1867. [[CrossRef](#)]
138. Lan, K.; Wang, X.; Yang, H.; Iqbal, K.; Zhu, Y.; Jiang, P.; Tang, Y.; Yang, Y.; Gao, W.; Li, R. Ultrafine MoP Nanoparticles Well Embedded in Carbon Nanosheets as Electrocatalyst with High Active Site Density for Hydrogen Evolution. *ChemElectroChem* **2018**, *5*, 2256–2262. [[CrossRef](#)]
139. Yu, Y.; Guo, Z.; Peng, Q.; Zhou, J.; Sun, Z. Novel two-dimensional molybdenum carbides as high capacity anodes for lithium/sodium-ion batteries. *J. Mater. Chem. A* **2019**, *7*, 12145–12153. [[CrossRef](#)]
140. Jiao, Y.; Zheng, Y.; Davey, K.; Qiao, S.-Z. Activity origin and catalyst design principles for electrocatalytic hydrogen evolution on heteroatom-doped graphene. *Nat. Energy* **2016**, *1*, 16130. [[CrossRef](#)]
141. Jiang, H.; Gu, J.; Zheng, X.; Liu, M.; Qiu, X.; Wang, L.; Li, W.; Chen, Z.; Ji, X.; Li, J. Defect-rich and ultrathin N doped carbon nanosheets as advanced trifunctional metal-free electrocatalysts for the ORR, OER and HER. *Energy Environ. Sci.* **2019**, *12*, 322–333. [[CrossRef](#)]

142. Chi, J.; Zeng, X.; Shang, X.; Dong, B.; Chai, Y.; Liu, C.; Marin, M.; Yin, Y. Embedding RhP_x in N, P Co-Doped Carbon Nanoshells Through Synergetic Phosphorization and Pyrolysis for Efficient Hydrogen Evolution. *Adv. Funct. Mater.* **2019**, *29*, 1901790. [[CrossRef](#)]
143. Lu, Z.; Wang, J.; Huang, S.; Hou, Y.; Li, Y.; Zhao, Y.; Mu, S.; Zhang, J.; Zhao, Y. N,B-codoped defect-rich graphitic carbon nanocages as high performance multifunctional electrocatalysts. *Nano Energy* **2017**, *42*, 334–340. [[CrossRef](#)]
144. Huang, S.; Meng, Y.; Cao, Y.; He, S.; Li, X.; Tong, S.; Wu, M. N-, O- and P-doped Hollow Carbons: Metal-free Bifunctional Electrocatalysts for Hydrogen Evolution and Oxygen Reduction Reactions. *Appl. Catal. B* **2019**, *248*, 239–248. [[CrossRef](#)]
145. Weng, B.; Grice, C.R.; Meng, W.; Guan, L.; Xu, F.; Yu, Y.; Wang, C.; Zhao, D.; Yan, Y. Metal–Organic Framework-Derived CoWP@C Composite Nanowire Electrocatalyst for Efficient Water Splitting. *ACS Energy Lett.* **2018**, *3*, 1434–1442. [[CrossRef](#)]
146. Wu, A.; Gu, Y.; Xie, Y.; Tian, C.; Yan, H.; Wang, D.; Zhang, X.; Cai, Z.; Fu, H. Effective Electrocatalytic Hydrogen Evolution in Neutral Medium Based on 2D MoP/MoS₂ Heterostructure Nanosheets. *ACS Appl. Mater. Interfaces* **2019**, *11*, 25986–25995. [[CrossRef](#)] [[PubMed](#)]
147. Zhao, W.J.; Li, M.Y.; Wu, H.M.; Feng, C.Q.; Zhang, G.X. Rod-like nonstoichiometric Ni_{0.85}Se as efficient electrocatalysts for hydrogen evolution reaction. *Int. J. Hydrogen Energy* **2018**, *43*, 12653–12660. [[CrossRef](#)]
148. Chi, J.; Chai, Y.; Shang, X.; Dong, B.; Liu, C.; Zhang, W.; Jin, Z. Heterointerface engineering of trilayer-shelled ultrathin MoS₂/MoP/N-doped carbon hollow nanobubbles for efficient hydrogen evolution. *J. Mater. Chem. A* **2018**, *6*, 24783–24792. [[CrossRef](#)]
149. Li, M.X.; Zhu, Y.; Wang, H.Y.; Wang, C.; Pinna, N.; Lu, X.F. Ni strongly coupled with Mo₂C encapsulated in nitrogen-doped carbon nanofibers as robust bifunctional catalyst for overall water splitting. *Adv. Energy Mater.* **2019**, *9*, 1803185–1803196. [[CrossRef](#)]
150. Liu, X.; Ni, K.; Niu, C.; Guo, R.; Xi, W.; Wang, Z.; Meng, J.; Li, J.; Zhu, Y.; Wu, P.; et al. Upraising the O 2p Orbital by Integrating Ni with MoO₂ for Accelerating Hydrogen Evolution Kinetics. *ACS Catal.* **2019**, *9*, 2275–2285. [[CrossRef](#)]
151. Yang, X.; Lu, A.Y.; Zhu, Y.; Min, S.; Hedhili, M.N.; Han, Y.; Huang, K.W.; Li, L.J. Rugae-like FeP nanocrystal assembly on a carbon cloth: An exceptionally efficient and stable cathode for hydrogen evolution. *Nanoscale* **2015**, *7*, 10974–10981. [[CrossRef](#)] [[PubMed](#)]
152. Xu, B.; Chen, Z.M.; Zhang, H.J.; Sun, Y.Q.; Li, C.C. Novel Ni(S_{0.49}Se_{0.51})₂ porous flakes array on carbon fiber cloth for efficient hydrogen evolution reaction. *Int. J. Hydrogen Energy* **2017**, *42*, 30119–30125. [[CrossRef](#)]
153. Bukola, S.; Merzougui, B.; Creager, S.E.; Qamarc, M.; Pederson, L.R.; Noui-Mehidi, M.N. Nanostructured cobalt-modified molybdenum carbides electrocatalysts for hydrogen evolution reaction. *Int. J. Hydrogen Energy* **2016**, *41*, 22899–22912. [[CrossRef](#)]
154. Ojha, K.; Saha, S.; Banerjee, S.; Ganguli, A.K. Efficient Electrocatalytic Hydrogen Evolution from MoS₂-Functionalized Mo₂N Nanostructures. *ACS Appl. Mater. Interfaces* **2017**, *9*, 19455–19461. [[CrossRef](#)] [[PubMed](#)]
155. Zhang, X.; Du, Z.; Luo, X.; Sun, A.; Wu, Z.; Wang, D. Template-free fabrication of hierarchical MoS₂/MoO₂ nanostructures as efficient catalysts for hydrogen production. *Appl. Surf. Sci.* **2018**, *433*, 723–729. [[CrossRef](#)]
156. Huang, L.; Yang, Y.; Zhang, C.; Yu, H.; Wang, T.; Dong, X.; Li, D.; Liu, Z. A nanostructured MoO₂/MoS₂/MoP heterojunction electrocatalyst for the hydrogen evolution reaction. *Nanotechnology* **2020**, *31*, 225403. [[CrossRef](#)]
157. Tang, Y.J.; Gao, M.R.; Liu, C.H.; Li, S.L.; Jiang, H.L.; Lan, Y.Q.; Han, M.; Yu, S.H. Porous molybdenum-based hybrid catalysts for highly efficient hydrogen evolution. *Angew. Chem. Int. Ed.* **2015**, *54*, 12928–12932. [[CrossRef](#)]
158. Zheng, D.; Feng, H.; Zhang, X.; He, X.; Yu, M.; Lu, X.; Tong, Y. Porous MoO₂ nanowires as stable and high-rate negative electrodes for electrochemical capacitors. *Chem. Commun.* **2017**, *53*, 3929–3932. [[CrossRef](#)]
159. Jiang, P.; Yang, Y.; Shi, R.; Xia, G.; Chen, J.; Su, J.; Chen, Q. Pt-like electrocatalytic behavior of Ru–MoO₂ nanocomposites for the hydrogen evolution reaction. *J. Mater. Chem. A* **2017**, *5*, 5475–5485. [[CrossRef](#)]
160. Ha, D.-H.; Han, B.; Risch, M.; Giordano, L.; Yao, K.P.C.; Karayaylali, P.; Shao-Horn, Y. Activity and stability of cobalt phosphides for hydrogen evolution upon water splitting. *Nano Energy* **2016**, *29*, 37–45. [[CrossRef](#)]
161. Han, G.H.; Kim, H.; Kim, J.; Kim, J.; Kim, S.Y.; Ahn, S.H. Micro-nanoporous MoO₂@CoMo heterostructure catalyst for hydrogen evolution reaction. *Appl. Catal. B Environ.* **2020**, *270*, 118895. [[CrossRef](#)]
162. Subbaraman, R.; Tripkovic, D.; Chang, K.-C.; Strmcnik, D.; Paulikas, A.P.; Hirunsit, P.; Chan, M.; Greeley, J.; Stamenkovic, V.; Markovic, N.M. Trends in activity for the water electrolyser reactions on 3d M(Ni,Co,Fe,Mn) hydr(oxy)oxide catalysts. *Nat. Mater.* **2012**, *11*, 550–557. [[CrossRef](#)]
163. Yao, N.; Li, P.; Zhou, Z.; Zhao, Y.; Cheng, G.; Chen, S.; Luo, W. Hydrogen Evolution Reaction: Synergistically Tuning Water and Hydrogen Binding Abilities over Co₄N by Cr Doping for Exceptional Alkaline Hydrogen Evolution Electrocatalysis. *Adv. Energy Mater.* **2019**, *9*, 1902449. [[CrossRef](#)]
164. Chen, Z.B.; Cummins, D.; Reinecke, B.N.; Clark, E.; Sunkara, M.K.; Jaramillo, T.F. Core-shell MoO₃-MoS₂ nanowires for hydrogen evolution: A functional design for electrocatalytic materials. *Nano Lett.* **2011**, *11*, 4168–4175. [[CrossRef](#)]
165. Laursen, A.B.; Kegnæs, S.; Dahl, S.; Chorkendorff, I. Molybdenum sulfides-efficient and viable materials for electro- and photoelectrocatalytic hydrogen evolution. *Energy Environ. Sci.* **2012**, *5*, 5577–5591. [[CrossRef](#)]
166. Wang, D.; Zhang, X.; Bao, S.; Zhang, Z.; Fei, H.; Wu, Z. Phase engineering of amultiphasic 1T/2H MoS₂ catalyst for highly efficient hydrogen evolution. *J. Mater. Chem. A* **2017**, *5*, 2681–2688. [[CrossRef](#)]
167. Pető, J.; Ollár, T.; Vancsó, P.; Popov, Z.I.; Magda, G.Z.; Dobrik, G.; Hwang, C.Y.; Sorokin, P.B.; Tapasztó, L.; Hwang, C.Y.; et al. Spontaneous doping of the basal plane of MoS₂ single layers through oxygen substitution under ambient conditions. *Nat. Chem.* **2018**, *10*, 1246–1251. [[CrossRef](#)]

168. Tang, C.; Wang, W.; Sun, A.; Qi, C.; Zhang, D.; Wu, Z.; Wang, D. Sulfur-Decorated Molybdenum Carbide Catalysts for Enhanced Hydrogen Evolution. *ACS Catal.* **2015**, *5*, 6956–6963. [[CrossRef](#)]
169. Vrubel, H.; Merki, D.; Hu, X. Hydrogen Evolution Catalyzed by MoS₃ and MoS₂ Particles. *Energy Environ. Sci.* **2012**, *5*, 6136–6144. [[CrossRef](#)]
170. Gao, Q.; Zhao, X.; Xiao, Y.; Zhao, D.; Cao, M. A mild route to mesoporous Mo₂C-C hybrid nanospheres for high performance lithium-ion batteries. *Nanoscale* **2014**, *6*, 6151–6157. [[CrossRef](#)]
171. Zhao, Y.; Bo, X.; Guo, L. An efficient electrocatalysts for the hydrogen evolution reaction based on molybdenum dioxide nanoparticles embedded porous graphene nanocomposite. *Int. J. Hydrogen Energy* **2017**, *42*, 5569–5576. [[CrossRef](#)]